

Highly Efficient Photocatalytic Reduction of CO₂ to CO under Visible Light Using Rhenium Benzo[d]Oxazole Complexes†

Uday Shee^a, Biswajit Khutia^a, Sneha Ray^a, Sumona Ghosh^a, Kajal Krishna Rajak^{a*}

^aInorganic Chemistry Section, Department of Chemistry, Jadavpur University, Kolkata- 700032, Email id: kajalk.rajak@jadavpuruniversity.in ; kajalrajak@rediffmail.com

Electronic Supplementary Information (ESI)

Table of Contents

	Page No.
<i>Experimental Section: Materials and Physical Measurements.</i>	S2-S4
<i>¹H NMR spectra and ¹³C spectra of the ligand 1a</i>	S5
<i>¹H NMR spectra and ¹³C spectra of the ligand 1b</i>	S6
<i>¹H NMR spectra and ¹³C spectra of the ligand 1c</i>	S7
<i>¹H NMR spectra and ¹³C spectra of the ligand 2a</i>	S8
<i>¹H NMR spectra and ¹³C spectra of the ligand 2b</i>	S9
<i>¹H NMR spectra and ¹³C spectra of the ligand 3a</i>	S10
<i>¹H NMR spectra and ¹³C spectra of the Complex-1a</i>	S11
<i>¹H NMR spectra and ¹³C spectra of the Complex-1b</i>	S12
<i>¹H NMR spectra and ¹³C spectra of the Complex-1c</i>	S13
<i>¹H NMR spectra and ¹³C spectra of the Complex-2a</i>	S14
<i>¹H NMR spectra and ¹³C spectra of the Complex-2b</i>	S15
<i>¹H NMR spectra and ¹³C spectra of the Complex-3a</i>	S16
<i>X-ray crystallographic data of the complexes</i>	S17-S21
<i>IR spectra of the complexes.</i>	S22
<i>Phosphorescence spectra of the Complexes.</i>	S23
<i>Emission decay curves of the complexes.</i>	S24
<i>Cyclic voltammetry data of the complexes</i>	S25
<i>TOF_{max} calculation from the CV data</i>	S26-S29
<i>Controlled potential electrolysis (CPE) data and faradaic efficiency data</i>	S29-S30
<i>Detection of gaseous products obtained from CPE</i>	S30
<i>Photocatalytic CO₂ reduction at different condition.</i>	S30-S31
<i>The amount of CO produced as a function of BIH concentration.</i>	S31
<i>A Stern-Volmer plots for the emission quenching by BIH</i>	S31-S34
<i>¹H NMR spectra for formic acid detection</i>	S35
<i>Photocatalytic reduction of CO₂ in bare sunlight</i>	S35
<i>GC-MS analysis for ¹³CO₂ leveling experiments.</i>	S36
<i>¹H spectrum during photocatalytic reaction</i>	S36
<i>TD-DFT experiment graph</i>	S37
<i>GC-TCD data for detection and amount calculation for CO</i>	S37
<i>References</i>	S38

Materials: Toluene, hexane, ethyl acetate, methanol, dichloromethane, *N,N*-dimethylformamide, and triethylamine were acquired from Mark and subjected to drying prior to use. 2-Picolylamine, 3,5-di-tert-butylcatechol, 2-picolinic acid, quinoline-2-carboxylic acid hydrochloride, 1-amino-2-naphthol hydrochloride, 3-amino-2-naphthol, Isoquinoline-1-carboxylic acid, 2,2,2-trifluoroethanol, 2,3-dihydro-1,3-dimethyl-2-phenylbenzimidazole(BIH), and pentacarbonylchlororhenium(I) were purchased from Sigma-Aldrich. Electrochemical-grade tetrabutylammonium hexafluorophosphate ($[n\text{Bu}_4\text{N}]\text{PF}_6$) with a minimum purity of 99.0% was also obtained from Sigma-Aldrich.

Instrumentation Details:

X-Ray crystallography:

The X-ray intensity data were recorded on Bruker AXS SMART APEX CCD diffractometer (Mo K_α , $\lambda = 0.71073 \text{ \AA}$) at 293 K. A total of 606 frames were collected with a scan width of 0.3° in different settings of φ . The data were reduced in SAINTPLUS¹ and empirical absorption correction was applied using the SADABS package. Metal atom was located by Patterson method and the rest of the non-hydrogen atoms were emerged from successive Fourier synthesis. The structures were refined by full matrix least-square procedure on F^2 . All non-hydrogen atoms were refined anisotropically. All the calculations were performed using the SHELXTL V 6.14 program package². Molecular structure plots were drawn using the Oak Ridge thermal ellipsoid plot (Ortep)

Physical Measurements :

^1H NMR spectra were recorded on Bruker FT 300 MHz spectrometer, where tetramethylsilane (TMS) was used as an internal reference and DMSO-d_6 was used as solvent. Micromass Q-Tof YA 263 mass spectrometer and Bruker Maxis Q-Tof ESI-MS were used to record the Electro-spray ionization mass spectrometry (ESI-MS) of the molecules. Elemental analyses (C, H, and N) of the synthesized molecules were carried out using Perkin–Elmer 2400 series II analyser. IR spectra were measured by Perkin–Elmer L-0100 spectrophotometer. The X-ray intensity data were collected on Bruker AXS SMART APEX CCD. UV–Vis spectra were measured by using a Shimadzu UV-VIS Spectrophotometer: UV 19001. Fluorescence spectroscopic studies were performed by using Horiba Fluoromax-4 spectrofluorometer. Electrochemical measurements were accomplished with the help of CHI600E electrochemical analyser using glassy carbon electrode under nitrogen atmosphere. Tetrabutylammoniumhexafluorophosphate was used as a supporting electrolyte and potentials were referenced to the Standard Calomel Electrode without junction correction. The impedance measurements were carried out using CHI760E workstation (CHI

Instruments, USA) through a conventional three-electrode system. Quantum yield of the complexes was determined in freeze-pump-thaw-degassed solutions of the complexes using quinine sulphate and fluorescein in the same solvent as the standard [$\Phi_{std}=0.54$ at 298 K in 0.1 M H₂SO₄ at $\lambda_{ex}=350$ nm] by usual method. The quantum yields were calculated by using Eq. S1.

$$\Phi_r = \Phi_{std} \frac{A_{std} I_r \eta_r^2}{A_r I_{std} \eta_{std}^2} \quad \text{Eq.S1}$$

where Φ_r and Φ_{std} are the quantum yields of unknown and standard samples, A_r and A_{std} refer to the solution absorbances at the excitation wavelength (λ_{ex}), I_r and I_{std} are the integrated emission intensities, η_r and η_{std} are the refractive indices of the solvent. Time-correlated-single-photon-counting (TCSPC) measurements were performed for the luminescence decay of the complexes in acetonitrile and dichloromethane. The fluorescence decay data were collected on a Hamamatsu MCP photomultiplier (R3809) and were analysed by using IBH DAS6 software.

Gas Detection by Gas Chromatography (GC):

The gas evolved during BE was detected by using GC instrument of model no. 8860 (G2790A), serial no. CN2211C039 fitted with TCD. 500 μ l gases was syringed out by a gas tight syringe from the head space of the working chamber of the H cell and was injected into the inlet of the GC.

Computational Study:

The geometrical structures of the singlet ground state and triplet excited state of the synthesized Re complexes were optimized by the DFT method³ using B3LYP exchange correlation functional⁴ approach. The geometry of the Re complexes was fully optimized in solution phase (namely dichloromethane and acetonitrile) without any symmetry constraints. There was a good agreement between the theoretically modelled and experimental structures. Based on the optimized ground state geometry, both the absorption and emission properties in acetonitrile and dichloromethane solvent was calculated by time-dependent density functional theory (TDDFT)⁵ approaches related with the conductor-like polarizable continuum model (CPCM).⁶ We computed the lowest 50 singlet – singlet transition and the results obtained from the TD calculations were qualitatively very similar. The TDDFT approach had been established to be reliable for calculating spectral properties of many transition metal complexes.⁷ Due to the presence of electronic correlation in the TDDFT (B3LYP) method it can yield more accurate electronic excitation energies. Hence TDDFT had been shown to provide a reasonable spectral feature for the complexes of our examination. In the calculation, the quasi-relativistic pseudo potentials of Re atoms were predicted by using Hay and Wadt⁸ with 14 valence electrons [outer-core (5s²5p⁶) electrons and the (5d⁶) valence electrons] were employed, and a “double- ξ ” quality basis set LANL2DZ was adopted as the basis set for Re atoms. For H 6-31(g)

basis set was used and the 6-31+ G (d, p) basis set was used for C, N, O and Cl atoms for the optimization of the ground state and excited state geometries. Gauss View 5.1 software was utilized to originate the figures showing MOs and the difference density plots. All the calculations were performed with the Gaussian 09W software package.⁹

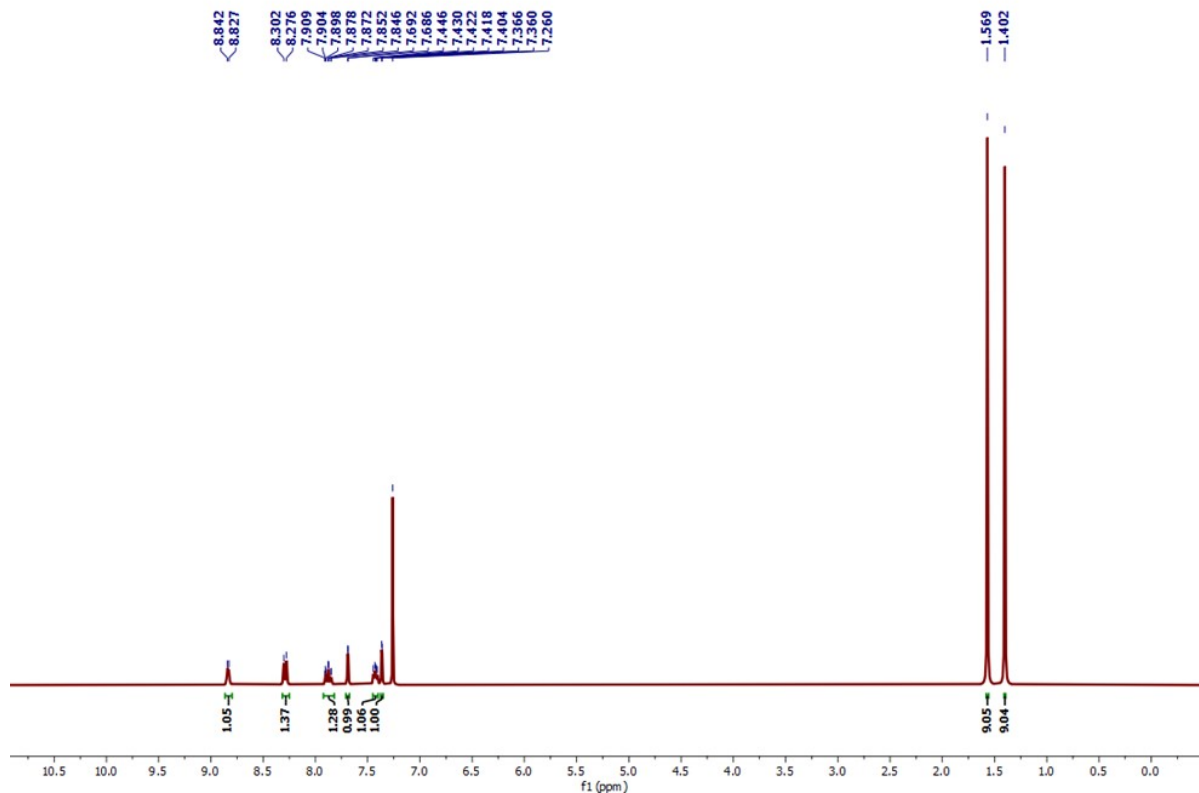


Fig. S1: ^1H NMR Spectrum of Ligand-1a in CDCl_3

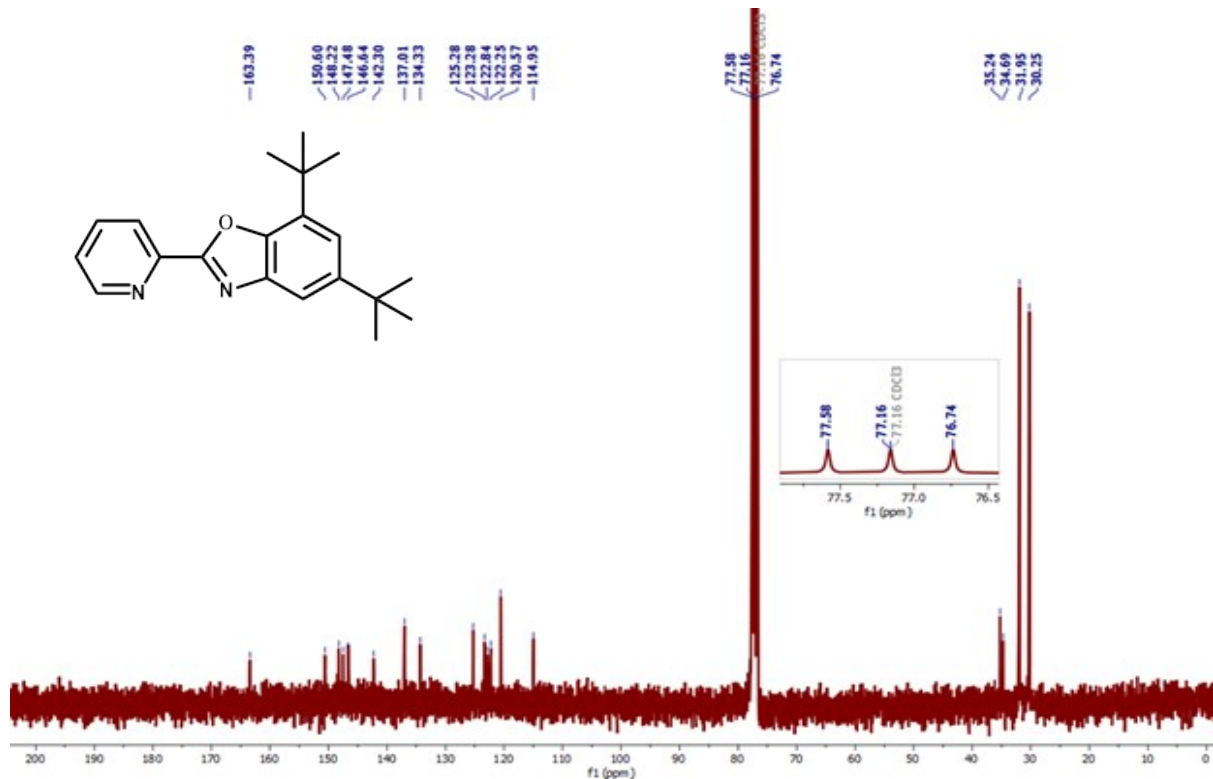


Fig. S2: ^{13}C NMR Spectrum of Ligand-1a in CDCl_3

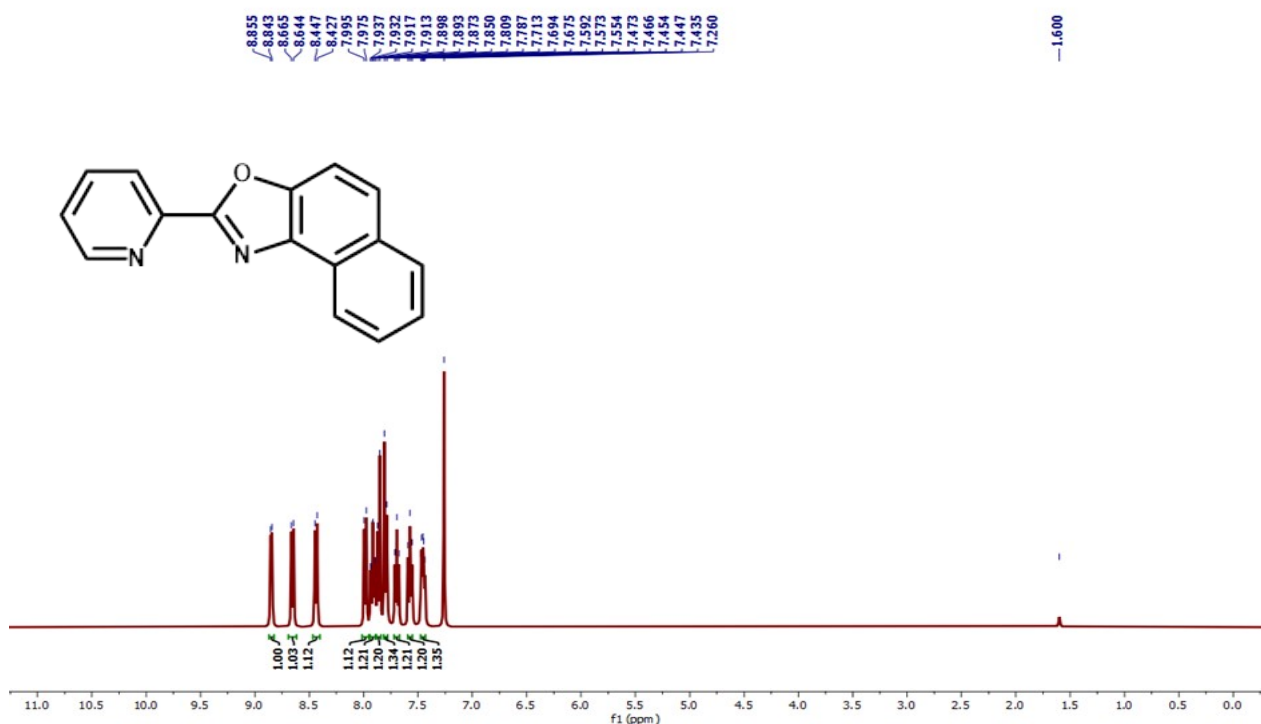


Fig. S3: ^1H NMR Spectrum of Ligand-1b in CDCl_3

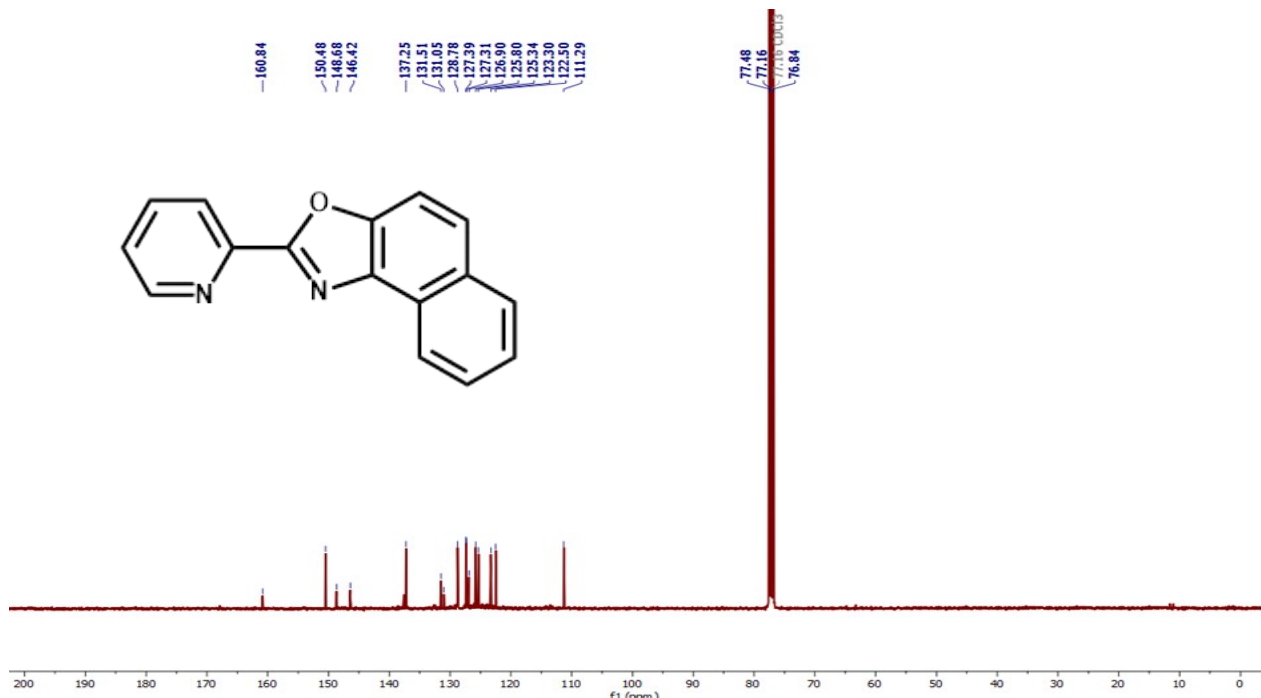


Fig. S4: ^{13}C NMR Spectrum of Ligand-1b in CDCl_3

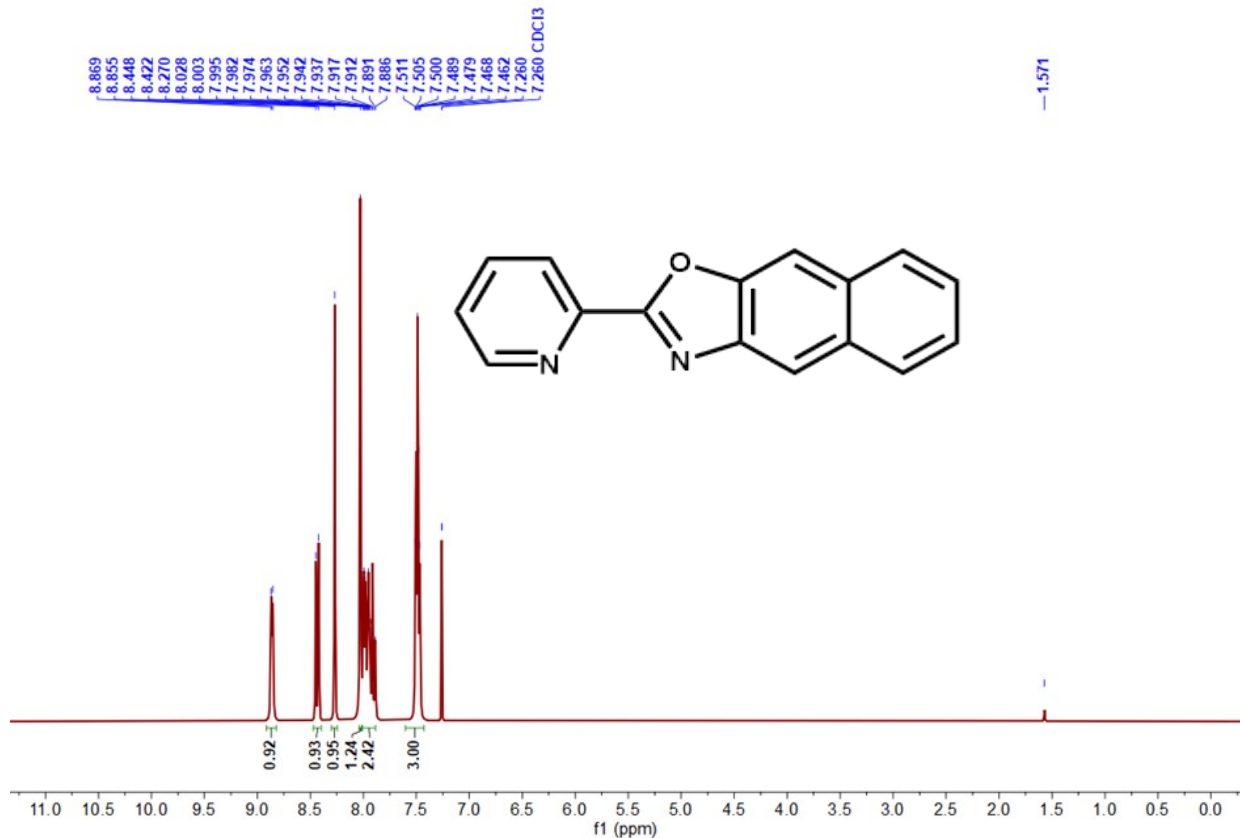


Fig. S5: ^1H NMR Spectrum of Ligand-1c in CDCl_3

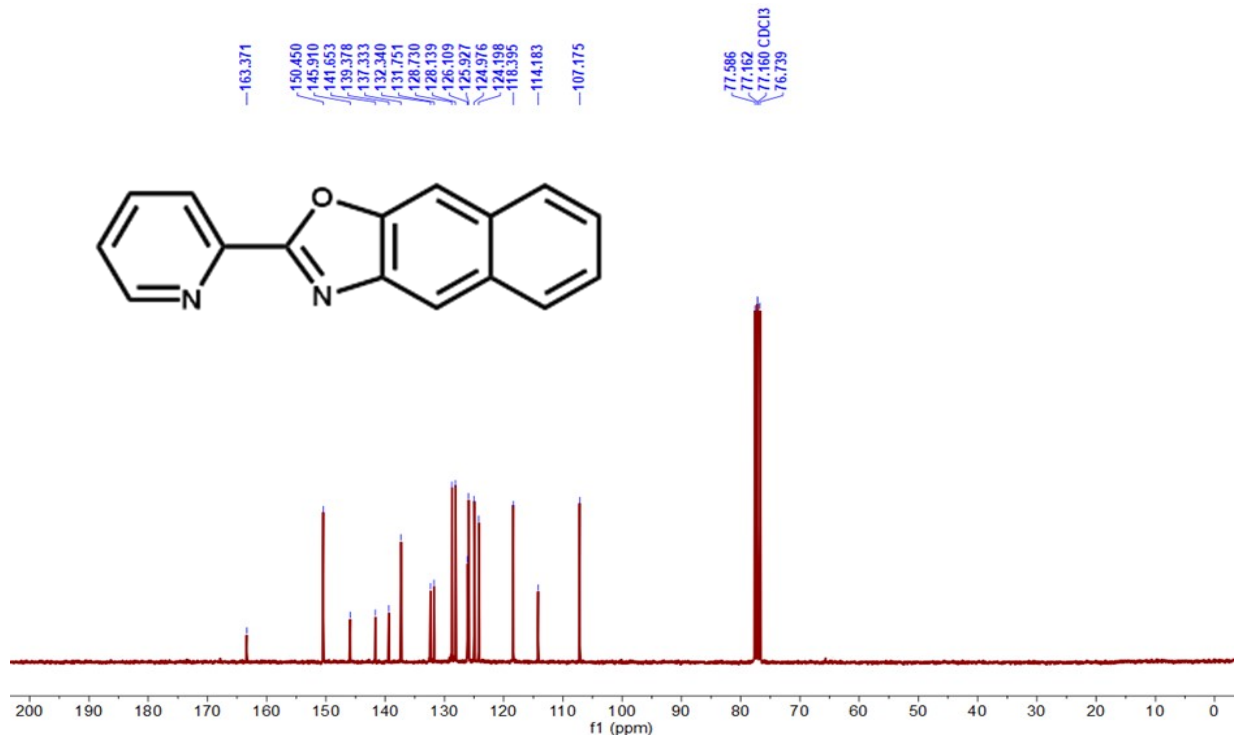


Fig. S6: ^{13}C NMR Spectrum of Ligand-1c in CDCl_3

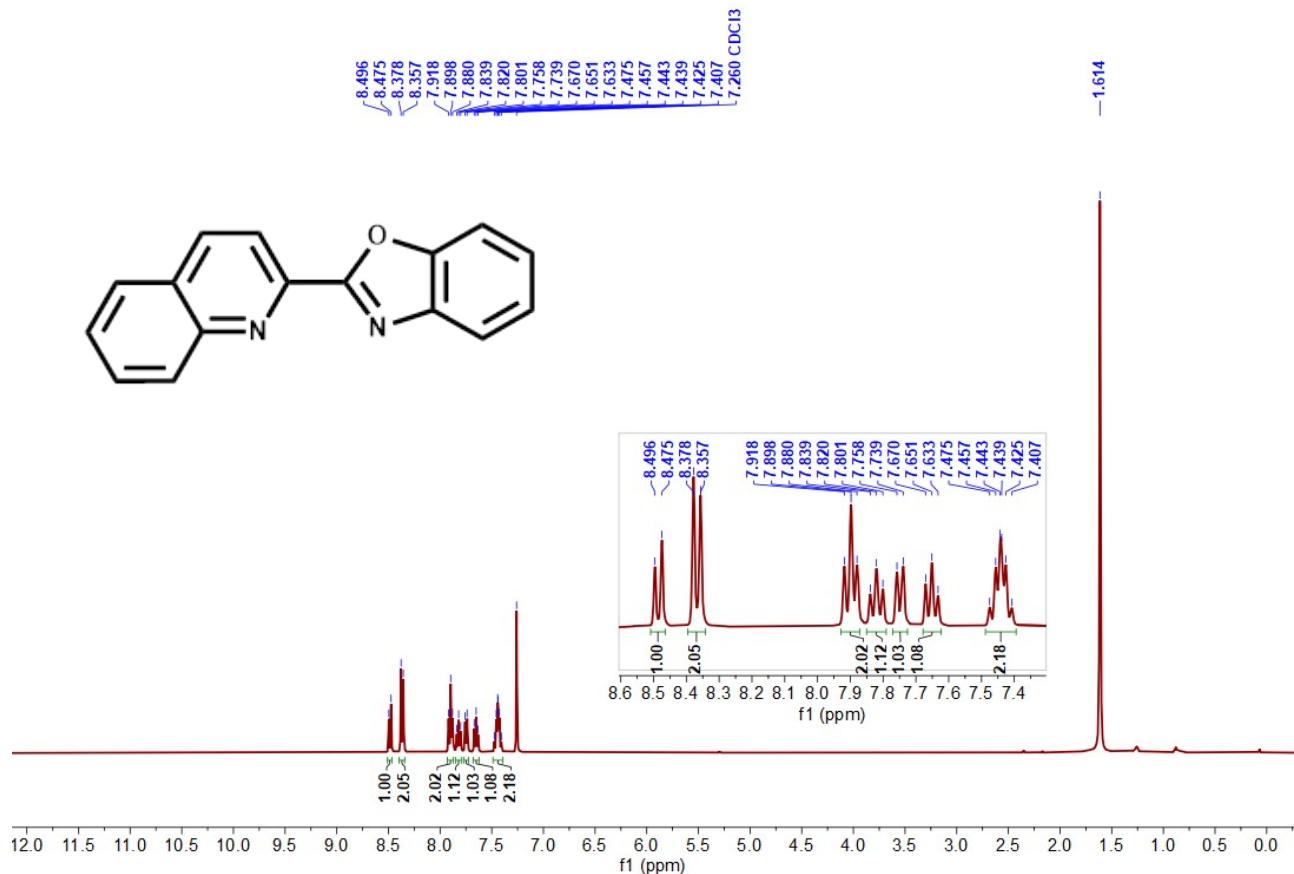


Fig. S7: ^1H NMR Spectrum of Ligand-2a in CDCl_3

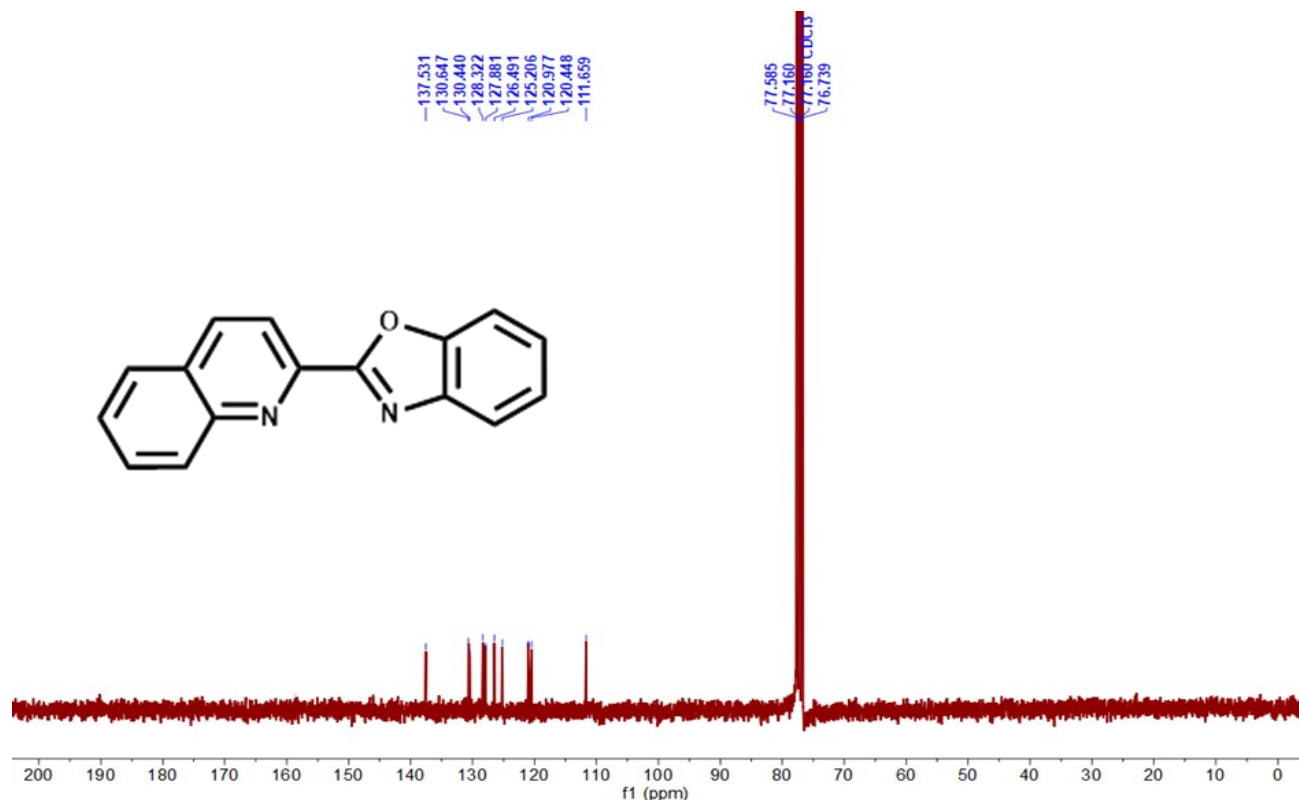


Fig. S8: ^{13}C NMR Spectrum of Ligand-2a in CDCl_3

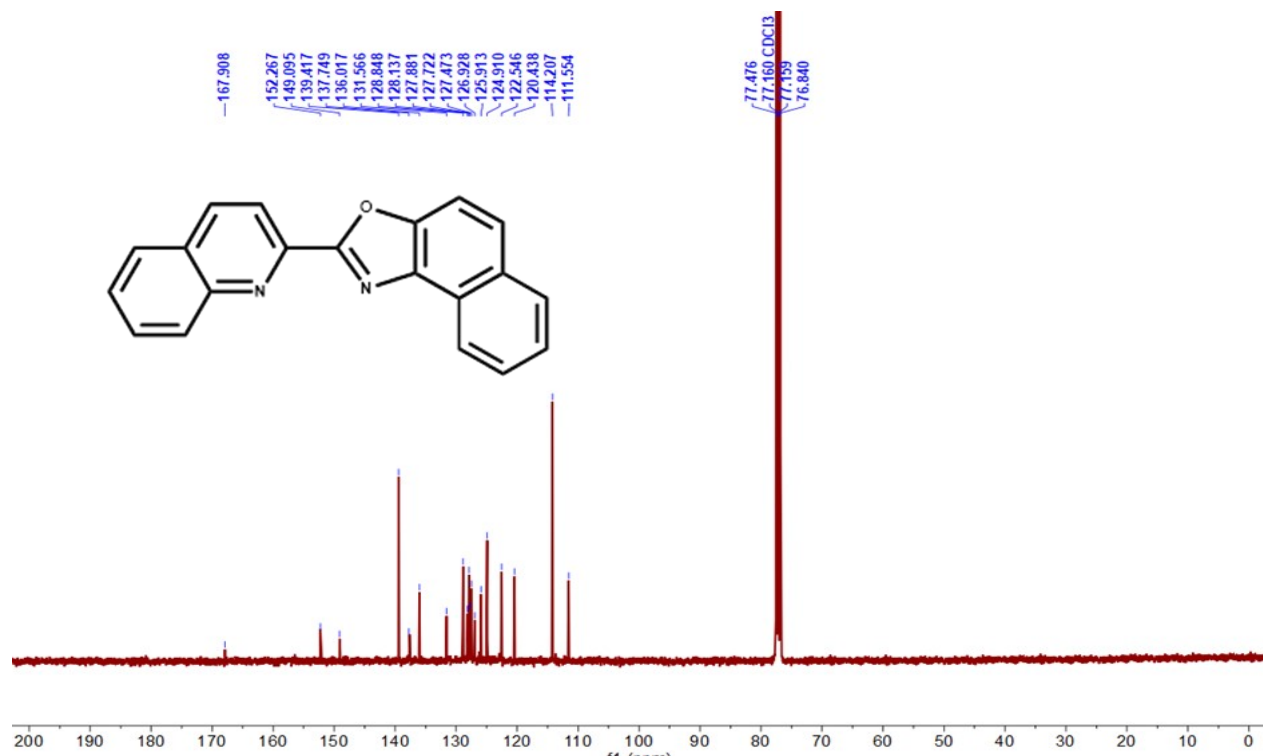
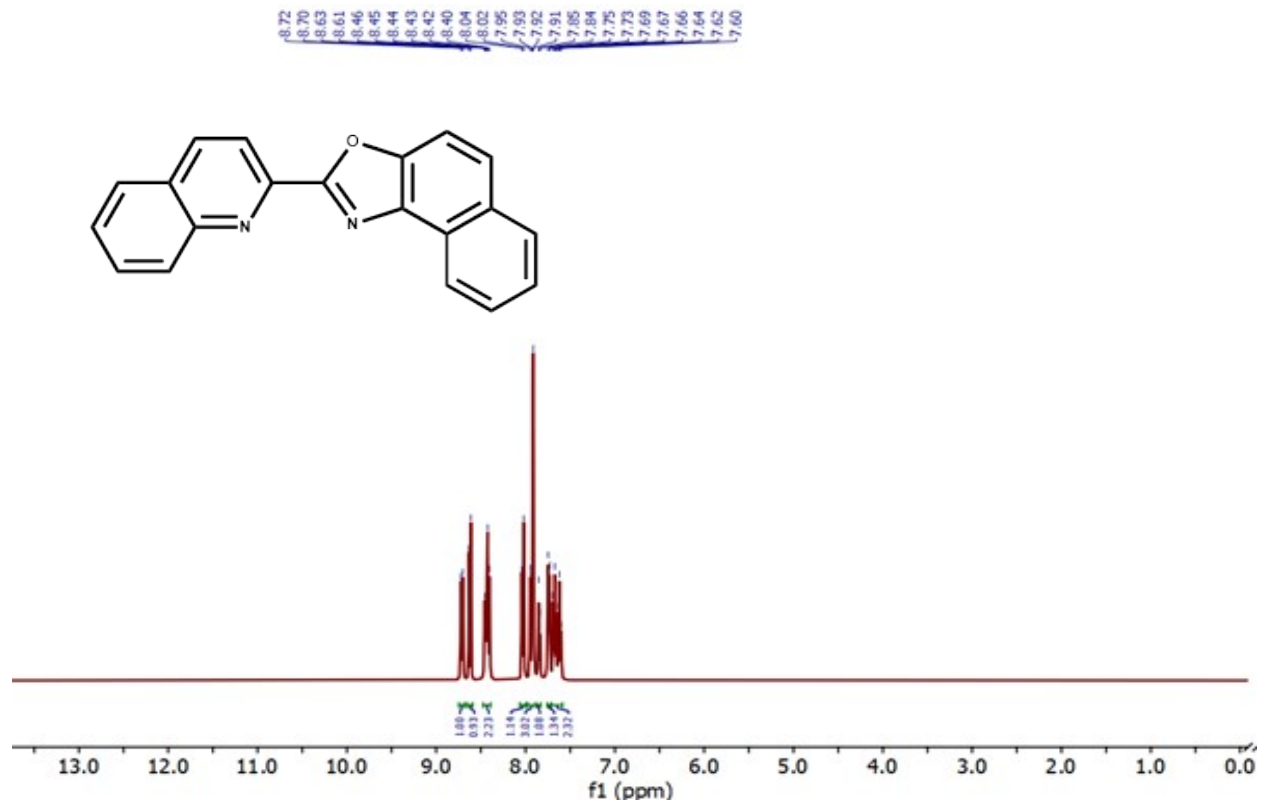


Fig. S9: ^1H NMR Spectrum of Ligand-2b in CDCl_3

Fig. S10: ^{13}C NMR Spectrum of Ligand-2b in CDCl_3

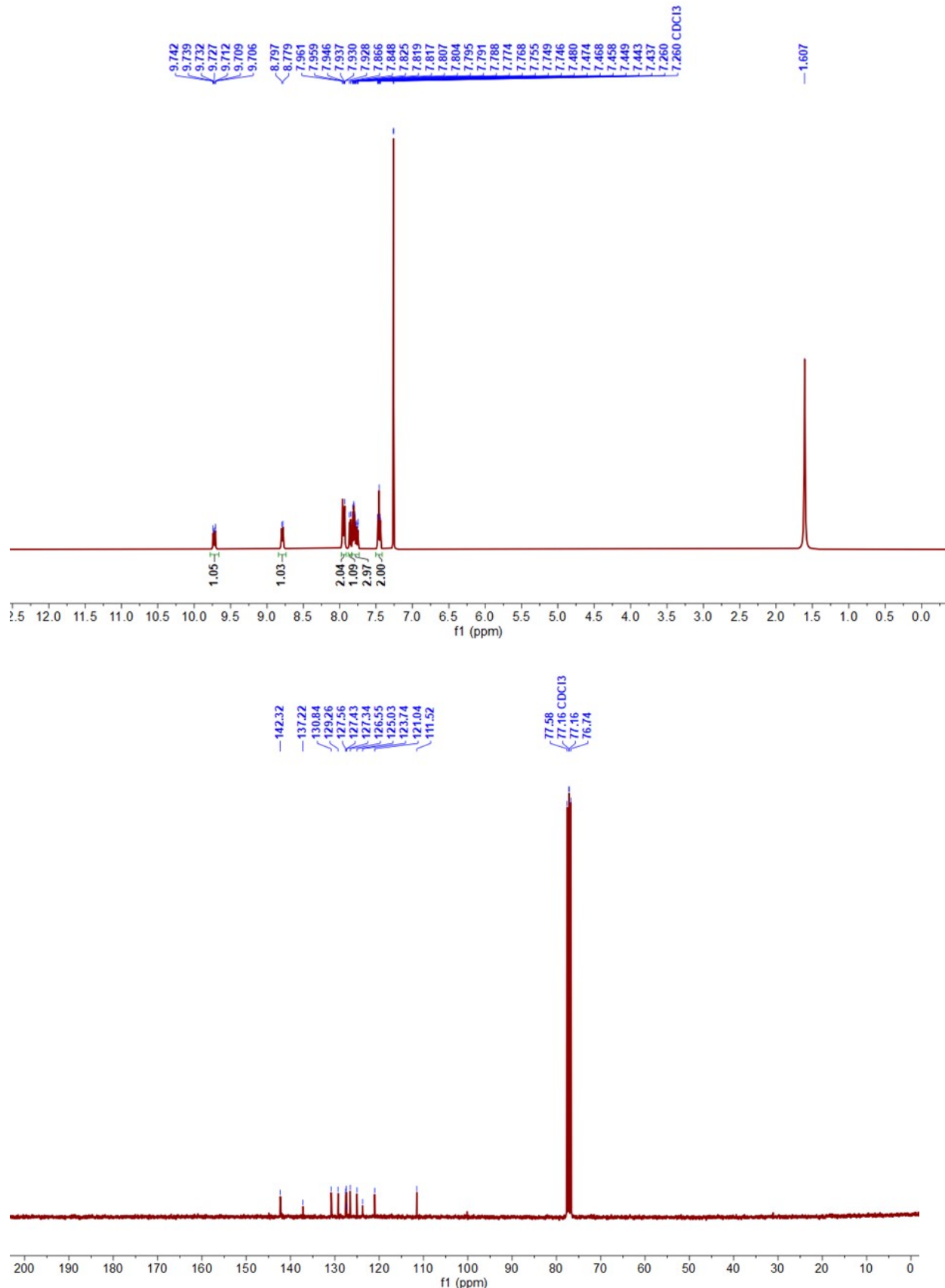
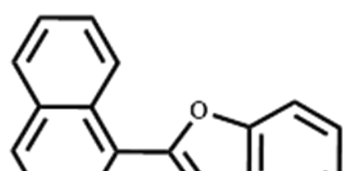


Fig. S11: ^1H NMR Spectrum of Ligand-3a in CDCl_3

Fig. S12: ^{13}C NMR Spectrum of Ligand-3a in CDCl_3



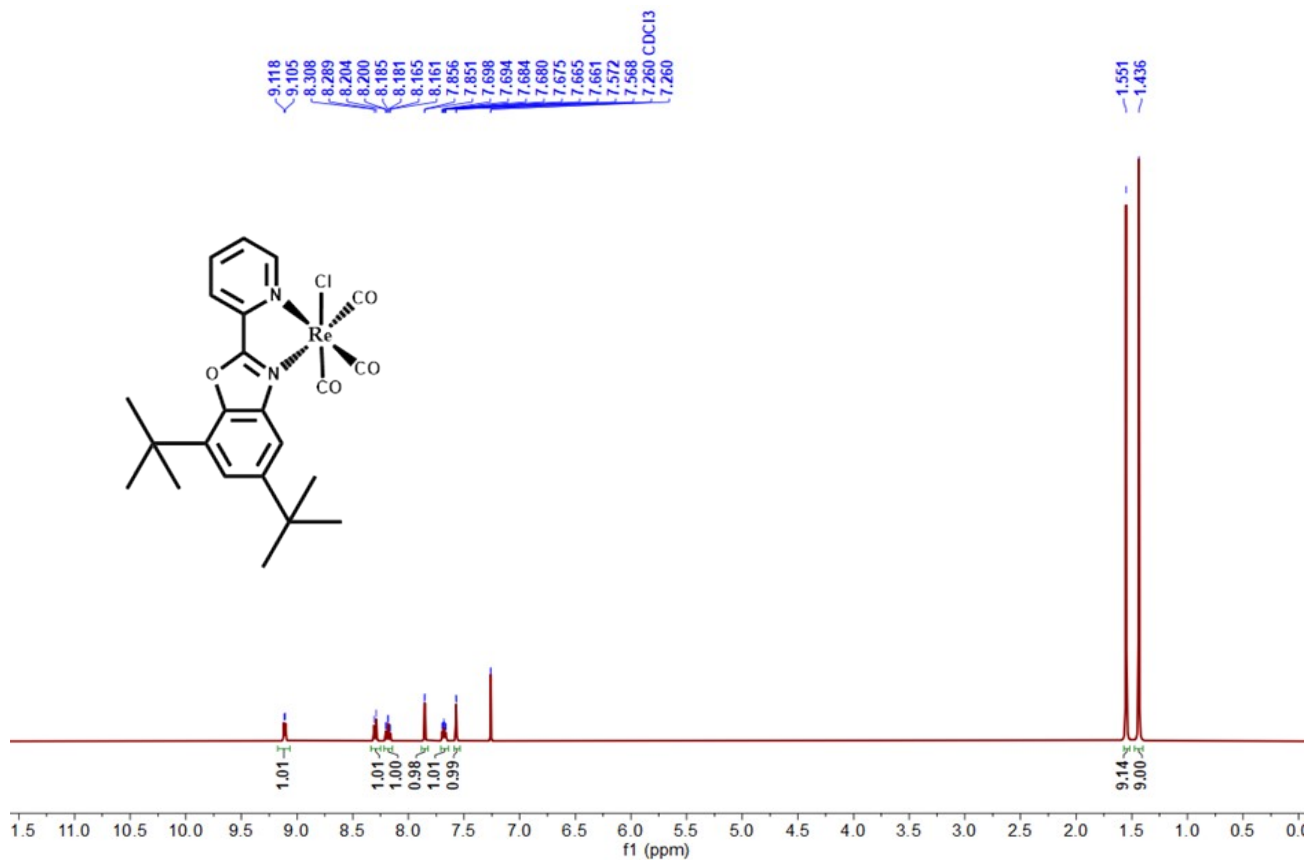


Fig. S13: ^1H NMR Spectrum of Complex-1a in CDCl_3

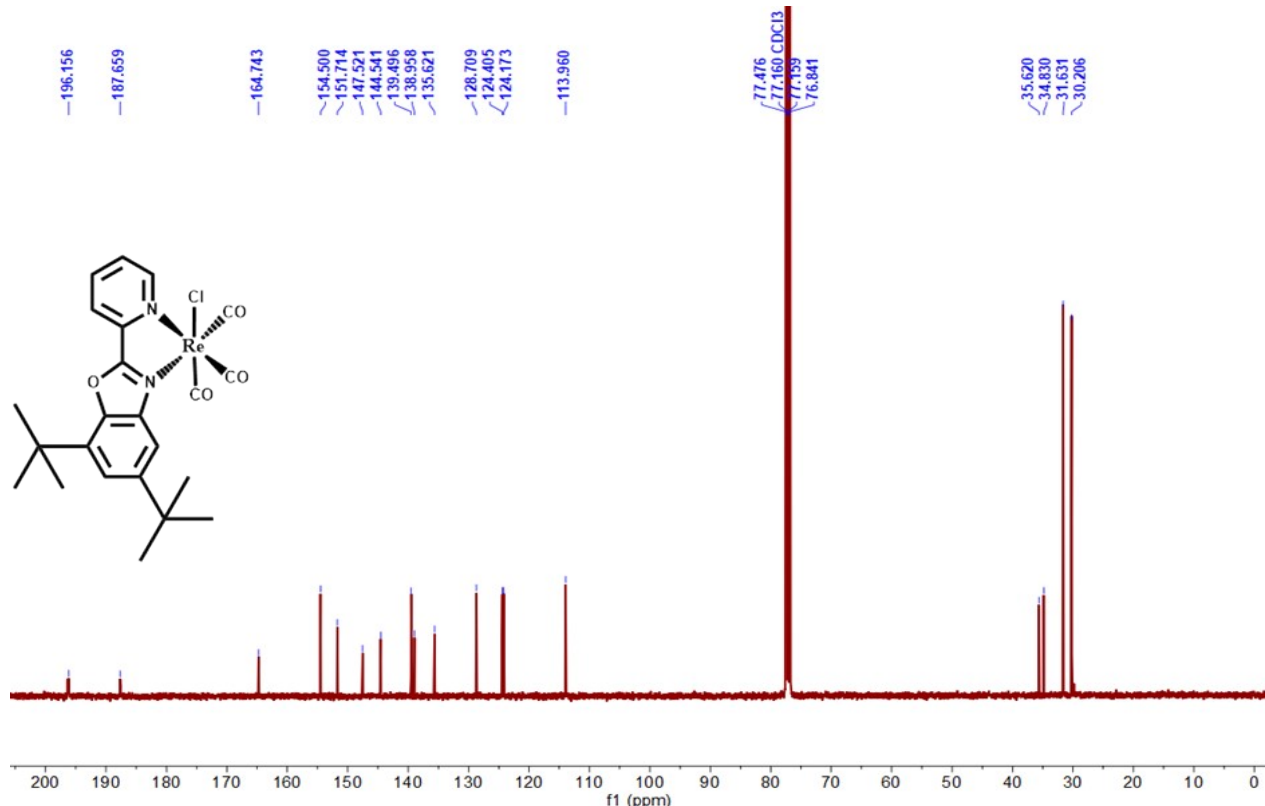


Fig. S14: ^{13}C NMR Spectrum of Complex-1a in CDCl_3 .

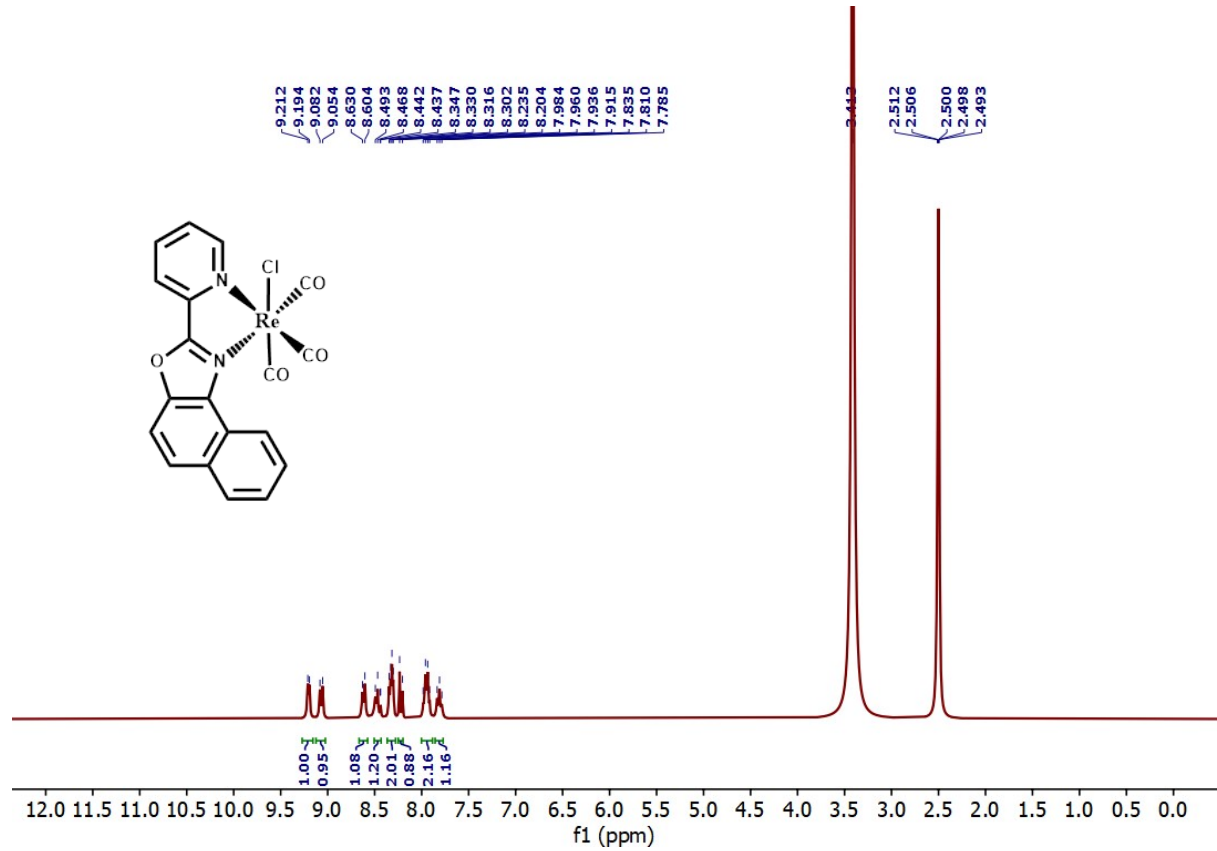


Fig. S15: ^1H NMR Spectrum of Complex-1b in DMSO-d_6

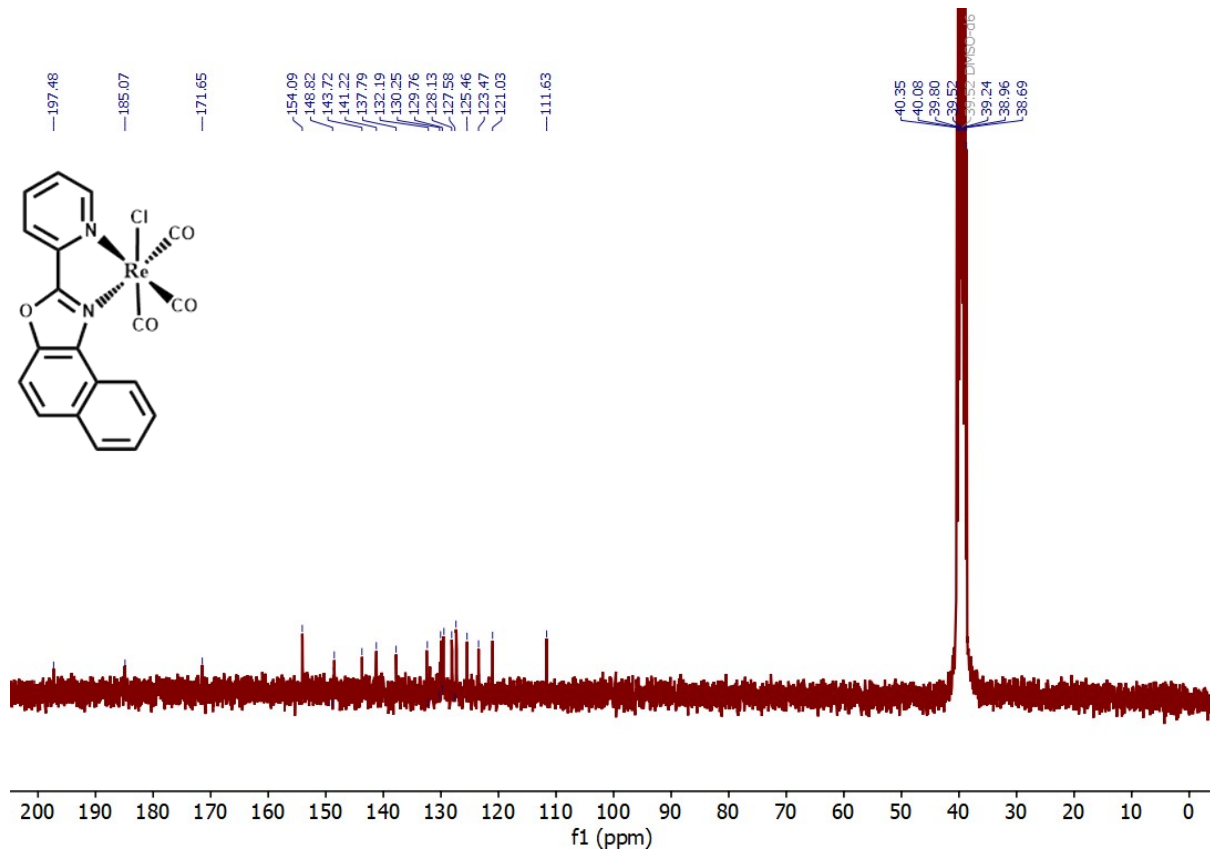


Fig. S16: ^{13}C NMR Spectrum of Complex-1b in DMSO-d_6

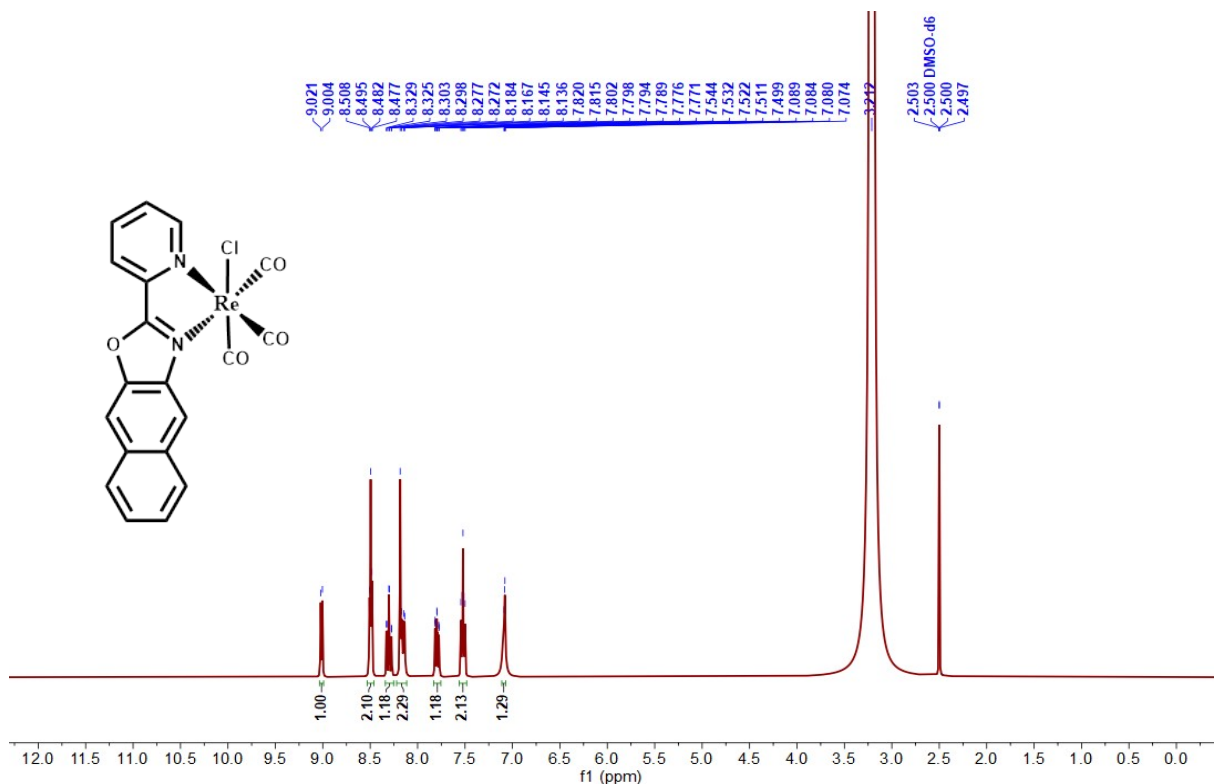


Fig. S17: ^1H NMR Spectrum of Complex-1c in DMSO-d_6

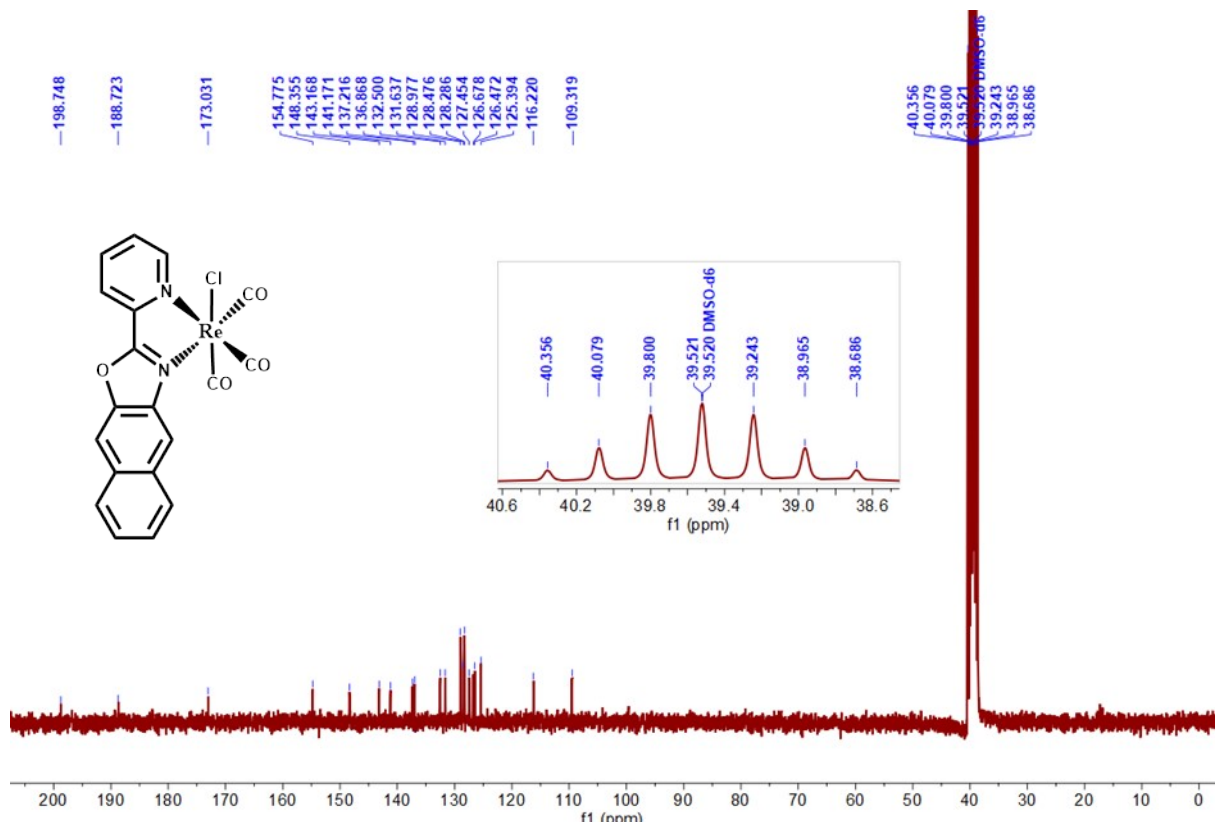


Fig. S18: ^{13}C NMR Spectrum of Complex-1c in DMSO-d_6

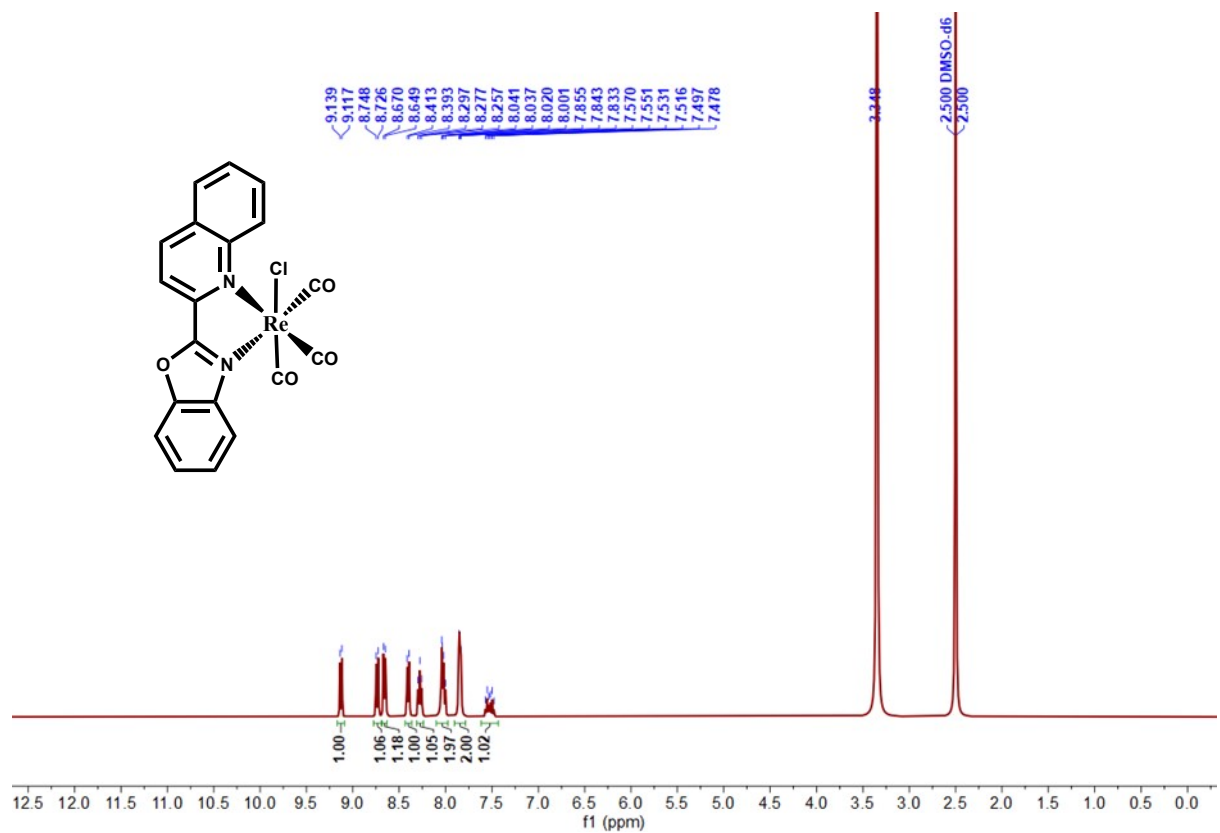


Fig. S19: ^1H NMR Spectrum of Complex-2a in DMSO-d_6

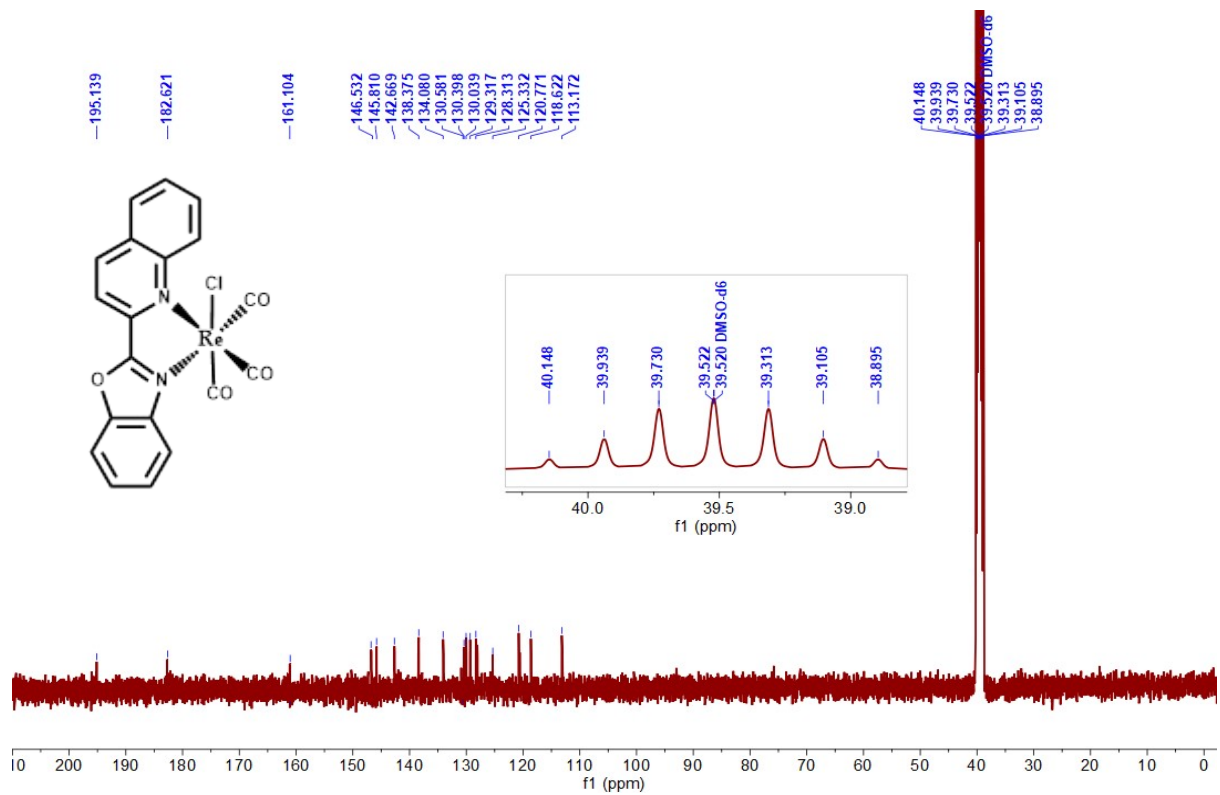


Fig. S20: ^{13}C NMR Spectrum of Complex-2a in DMSO-d_6

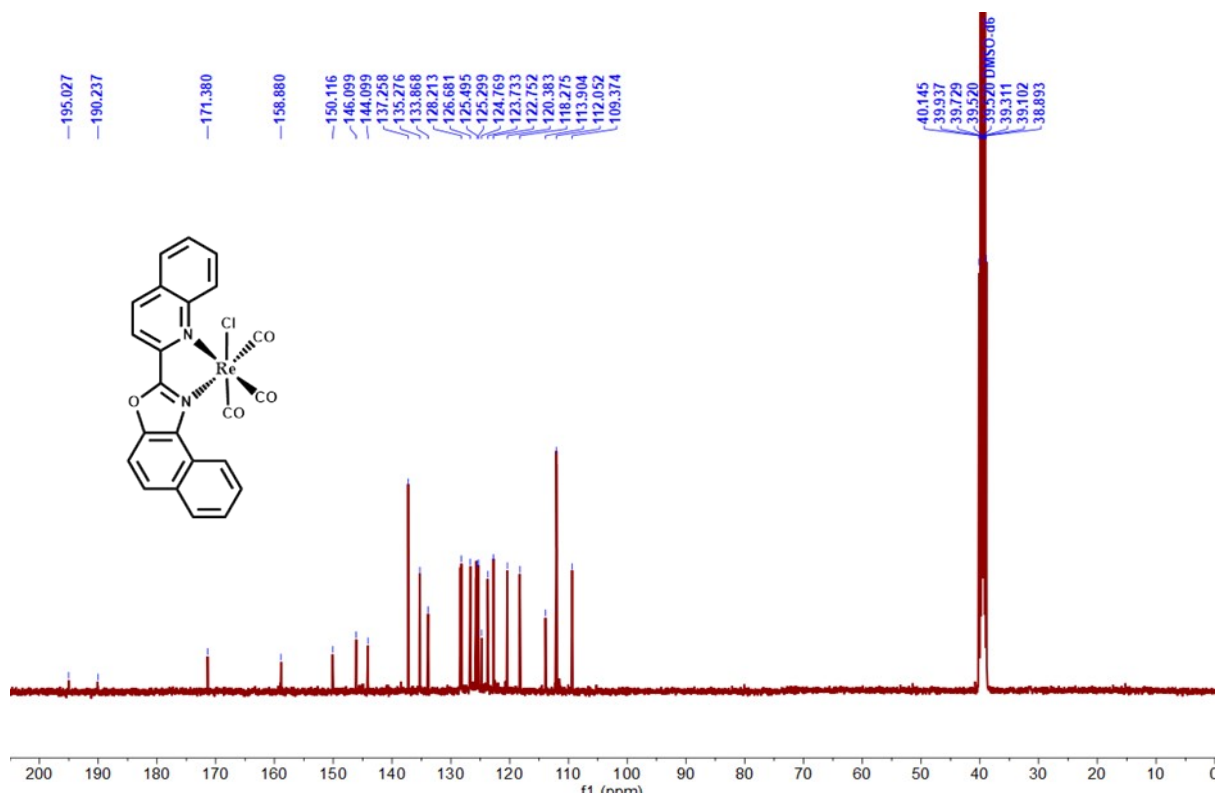
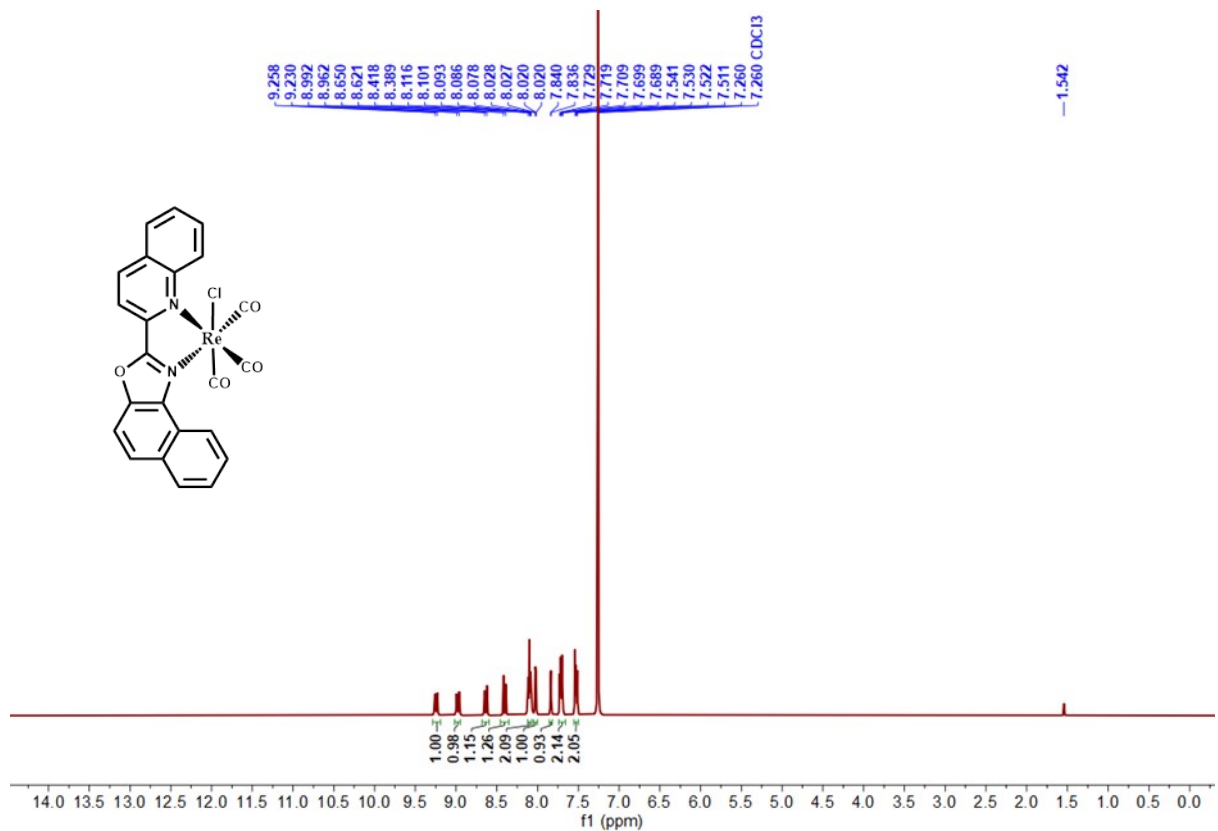


Fig. S21: ^1H NMR Spectrum of Complex-2b in DMSO- d_6 .

Fig. S22: ^{13}C NMR Spectrum of Complex-2b in DMSO- d_6

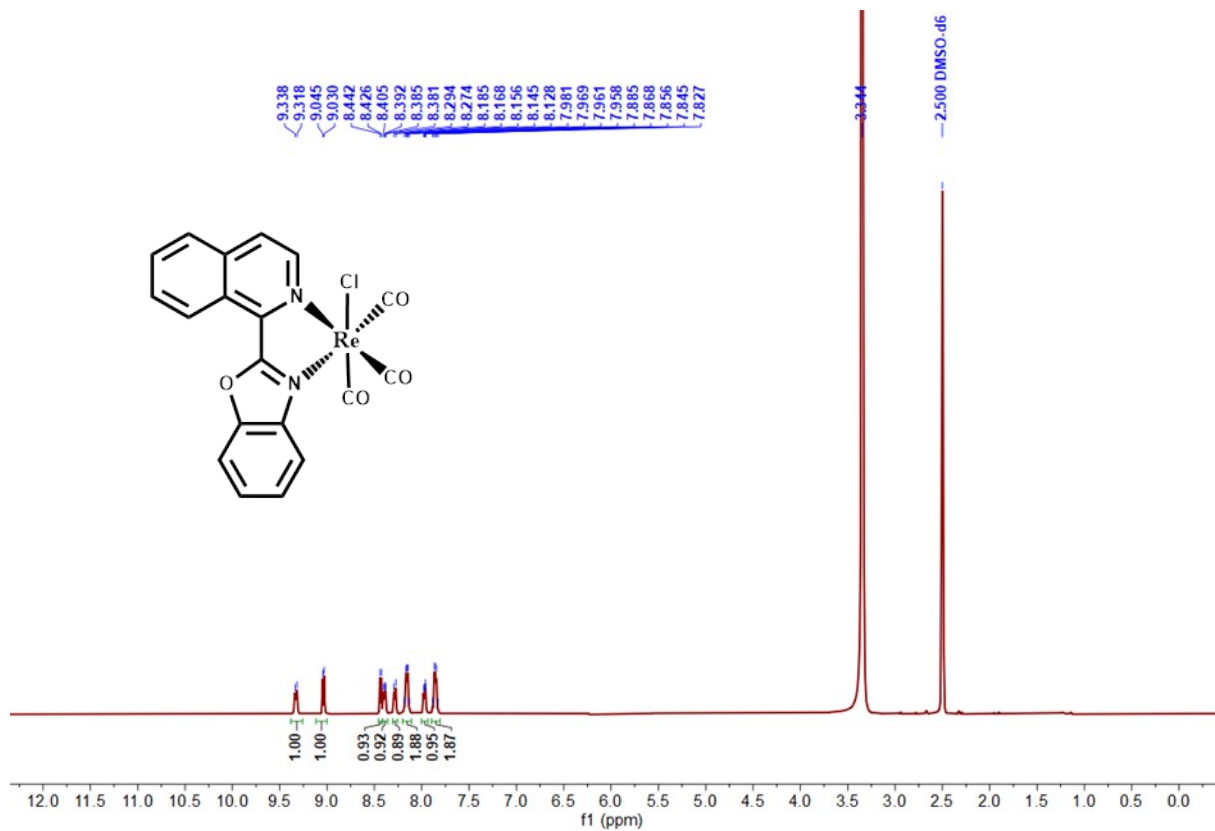


Fig. S23: ^1H NMR Spectrum of Complex-3a in DMSO-d_6 .

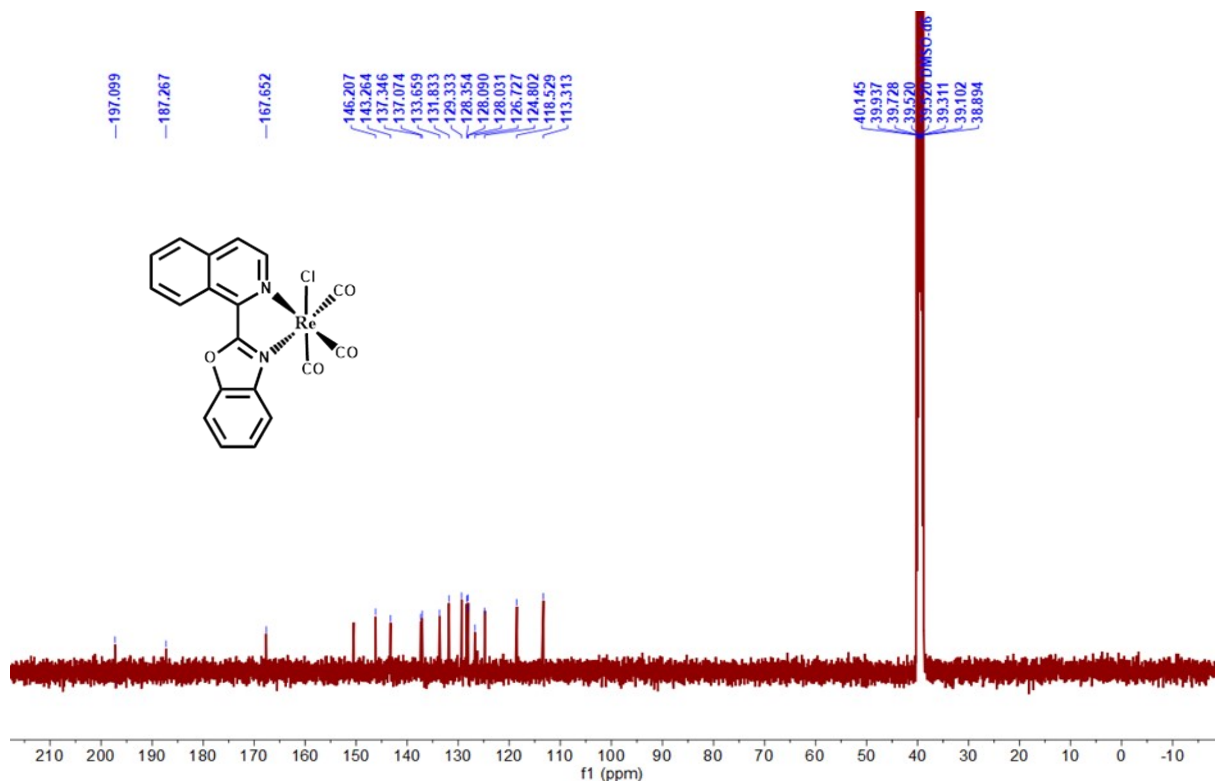


Fig. S24: ^{13}C NMR Spectrum of Complex-3a in DMSO-d_6

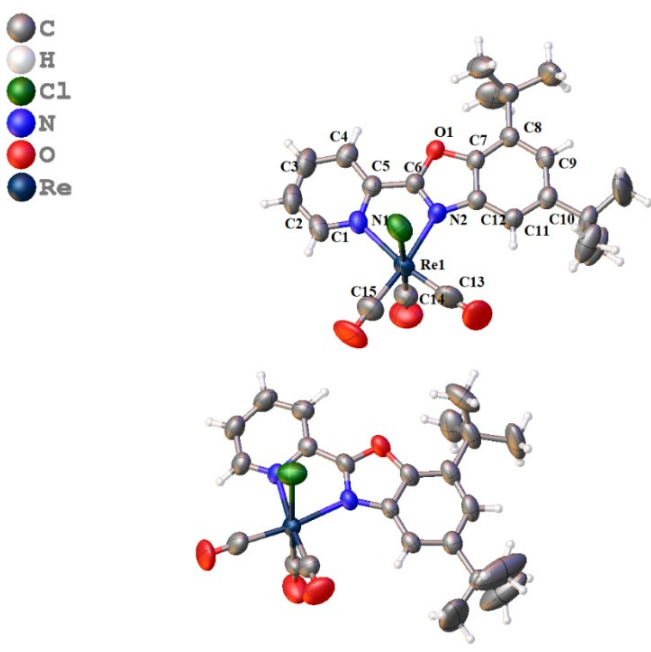
	Complex-1a	
	CCDC No. 2355624	
Formula		C_{45.75}H₄₈Cl₂N₄O₈Re₂
Molecular weight		1225.18
Crystal system		monoclinic
Space group		P 1 21/c 1
a/ Å	16.2390(11)	
b/ Å	11.9393(8)	
c/ Å	26.1931(17)	
α/°	90	
β/°	105.713(2)	
γ/°	90	
V/ Å³	4888.6(6)	
Z	4	
Dcalcd /g cm⁻³	1.665	
Bond length(Å)		Mu (mm-1) 5.110
Re-N1	2.213(4)	T/K 273.15
Re-N2	2.170(4)	R1 = 0.0316, wR2 = 0.0800
C6-O1	1.349(5)	
O1-C7	1.395(5)	GOF on F2 1.056
C6-N2	1.308(6)	
N2-C12	1.399(6)	

Table S1: crystallographic data of the **complex 1a**

Complex-1b		
CCDC No.	2385160	
Formula	C₁₉ H₁₀ Cl N₂ O₄ Re	
Molecular weight	551.94	
Crystal system	'triclinic'	
Space group	P -1	
a/ Å	6.977(5)	
b/ Å	9.781(7)	
c/ Å	13.71(1)	
α/°	86.855(19)	
β/°	75.528(18)	
γ/°	76.140(18)	
V/ Å³	879.5(11)	
Z	2	
Dealed /g cm⁻³	2.084	
Bond length(Å)	Mu (mm-1) 7.088	
Re-N1	2.211(6)	T/K 273
Re-N2	2.254(6)	R1 = 0.0488, wR2 = 0.1139
C6-O1	1.349(8)	
O1-C7	1.377(9)	GOF on F2 1.074
C6-N2	1.315(8)	
N2-C16	1.411(9)	

Table S2: crystallographic data of the **complex 1b**

Complex-1c			
CCDC No. 2385164			
Formula	$C_{19} H_{10} Cl N_2 O_4 Re$,		
1	$[CH_2Cl_2]$		
Molecular weight	636.87		
Crystal system	'triclinic'		
Space group	P -1		
a/ Å	9.4862(4)		
b/ Å	9.5540(4)		
c/ Å	13.1539(6)		
$\alpha/^\circ$	96.340(1)		
$\beta/^\circ$	102.856(1)		
$\gamma/^\circ$	110.709(1)		
V/ Å³	1063.54(8)		
Z	2		
Dealed /g cm⁻³	1.989		
Bond length(Å)			
Re-N1	2.205(3)	Mu/mm⁻¹	6.119
Re-N2	2.179(3)	T/K	273
C6-O1	1.352(5)	R1 = 0.0252,	
O1-C7	1.390(5)	wR2 = 0.0550	
C6-N2	1.293(5)	GOF on F2	0.983
N2-C16	1.417(5)		

Table S3: crystallographic data of the complex **1c**

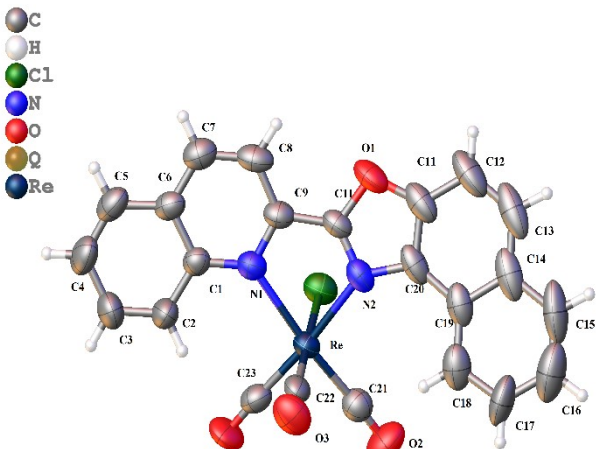
		
Complex-2b		
CCDC No.	<u>2385178</u>	
Formula	C₂₃ H₁₂ Cl N₂ O₄ Re	
Molecular weight	602.00	
Crystal system	'monoclinic'	
Space group	P -1	
a/ Å	7.2623(6)	
b/ Å	9.6207(7)	
c/ Å	14.8789(11)	
α/°	99.464(2)	
β/°	96.228(3)	
γ/°	100.601(2)	
V/ Å³	997.54(13)	
Z	2	
Dcalcd /g cm⁻³	2.004	
Bond length(Å)	Mu/mm⁻¹ 6.259	
Re-N1	2.279(6)	T/K 273
Re-N2	2.209(6)	R1 = 0.0400, wR2 = 0.1004
C10-O1	1.362(8)	
O1-C11	1.376(12)	GOF on F2 1.047
C10-N2	1.279(10)	
N2-C20	1.396(10)	

Table S4: crystallographic data of the **complex-2b**

Complex-3a	
CCDC No.	2385175
Formula	C₁₉ H₁₀ Cl N₂ O₄ Re
Molecular weight	551.94
Crystal system	'monoclinic'
Space group	'P 1 21/c 1'
a/ Å	8.3981(5)
b/ Å	16.0907(9)
c/ Å	13.2068(8)
α/°	90
β/°	93.733(2)
γ/°	90
V/ Å³	1780.87(18)
Z	4
Dcalcd /g cm⁻³	2.059
Bond length(Å)	Mu/mm⁻¹ 7.002
Re-N1	2.210(5)
Re-N2	2.158(4)
C10-O1	1.350(6)
O1-C11	1.391(6)
C10-N2	1.350(6)
N2-C16	1.401(7)
T/K 273	
R1 = 0.0346, wR2 = 0.0976	
GOF on F2 1.059	

Table S5: crystallographic data of the complex-3a

Vibrational Spectra

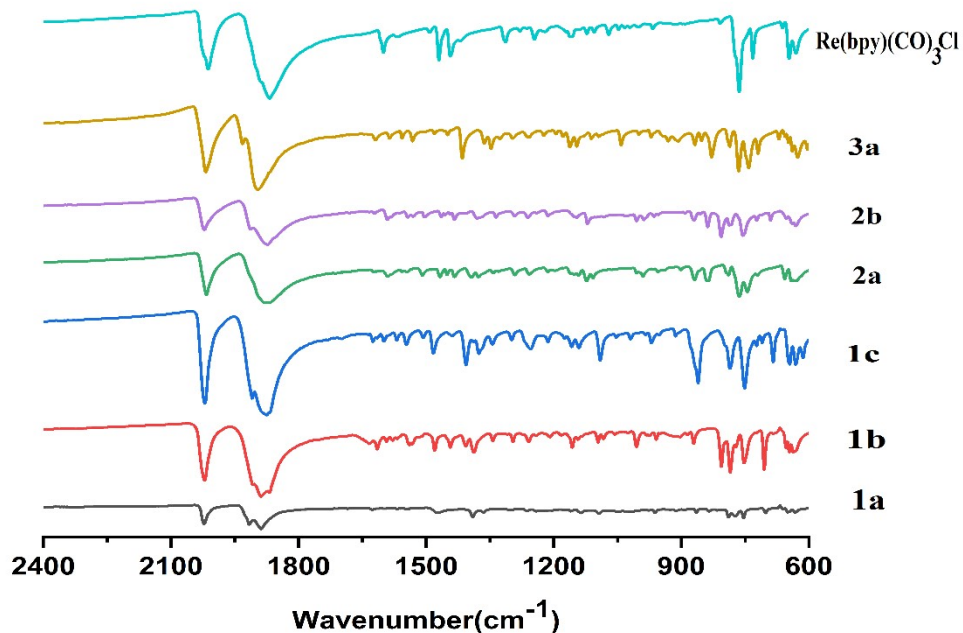


Fig. S25: FTIR Spectra of the complexes.

complex	experimental ν_{CO} (cm ⁻¹)
Re(bpy)(CO) ₃ Cl	2021, 1917, 1897
Complex-1a	2021, 1915, 1888
Complex-1b	2020, 1906, 1880
Complex-1c	2020, 1908, 1883
Complex-2a	2016, 1915, 1879
Complex-2b	2021, 1912, 1876
Complex-3a	2018, 1931, 1896

Table S6: IR stretching frequencies of the complexes.

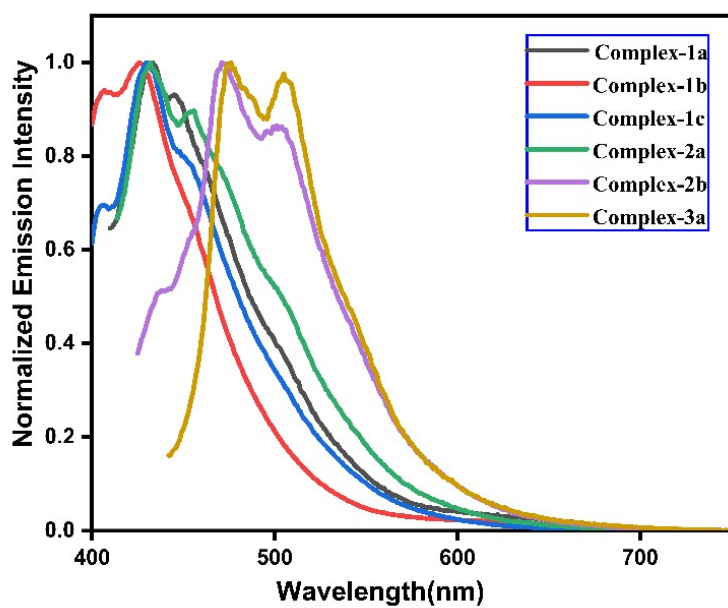


Fig. S26: Normalized Emission plots of the complexes (1a, 1b, 1c, 2a, 2b, 3a) recorded in CH_3CN at room temperature.

Complex	$\lambda_{\text{exc}}(\text{nm})$	$\lambda_{\text{emi}}(\text{nm})$	Φ_{EM}	$\tau_1(\text{ns})$	$\tau_2(\text{ns})$	$\tau_{\text{avg}}(\text{ns})$	$k_r(\text{s}^{-1}) \times 10^7$	$k_{\text{nr}}(\text{s}^{-1}) \times 10^8$
1a	400	431,446	0.11	1.32	7.73	4.17	1.4	1.15
1b	400	405,424	0.51	2.11	-	2.11	24.1	2.32
1c	402	429	0.24	1.54	7.72	5.27	3.1	0.98
2a	400	431,455	0.13	1.87	7.48	7.06	1.7	1.26
2b	416	471,501	0.07	2.02	-	2.02	3.4	4.6
3c	430	474,504	0.05	2.04	8.17	5.28	0.6	1.16

Table S7: Photophysical parameters of the complexes. All the complexes were excited at the maximum wavelength of absorption ($\lambda_{\text{max}} = \lambda_{\text{exc}}$)

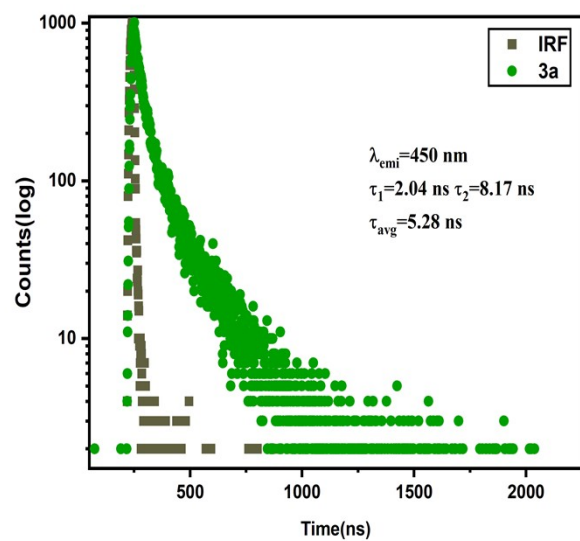
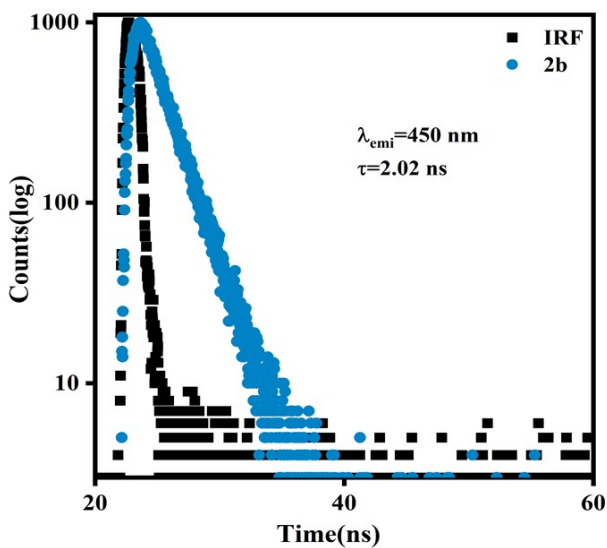
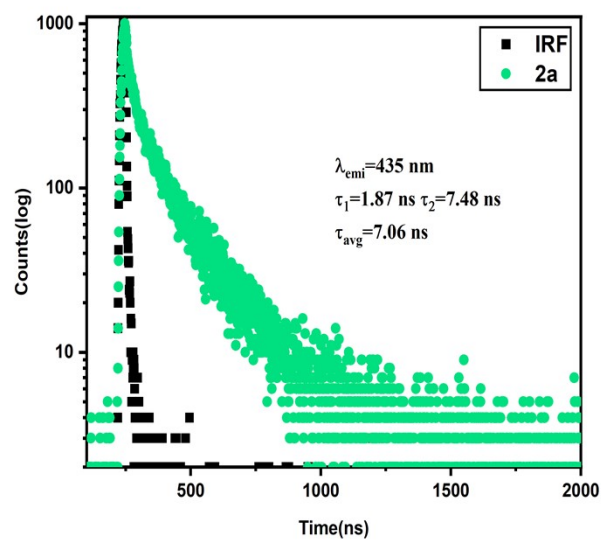
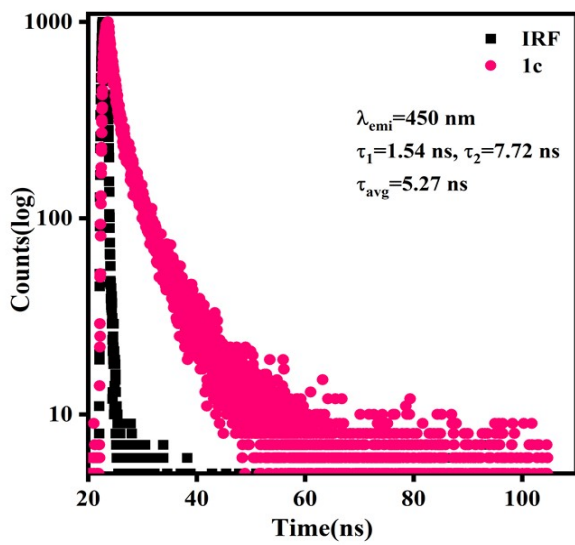
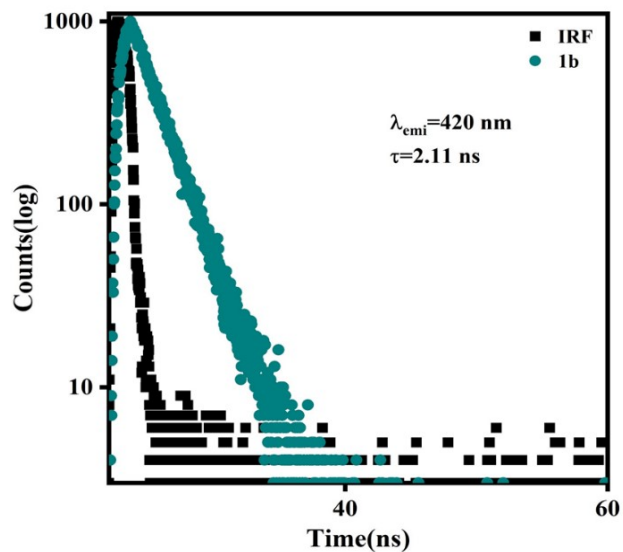
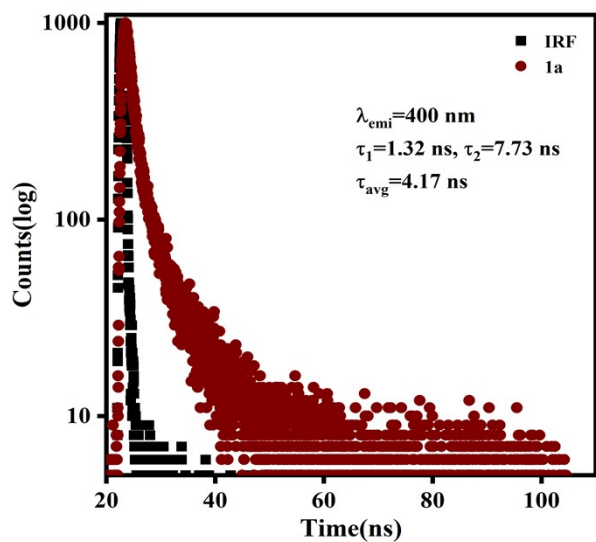
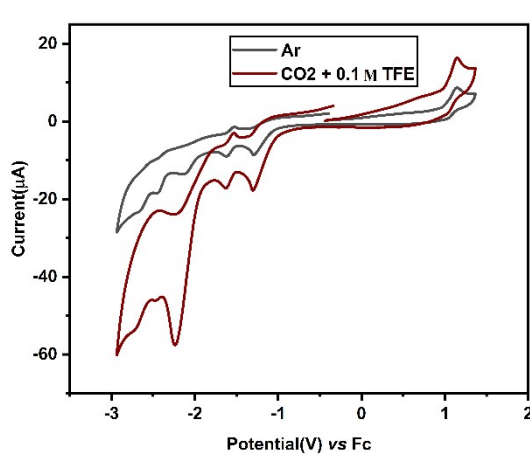


Fig. S27. Emission decay curves of **complex-1a, 1b, 1c, 2a, 2b and 3a** in aerated CH_3CN .

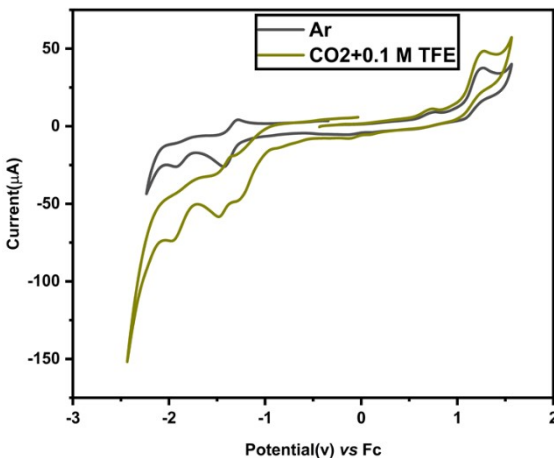


Electrochemistry

1a

2a

3a

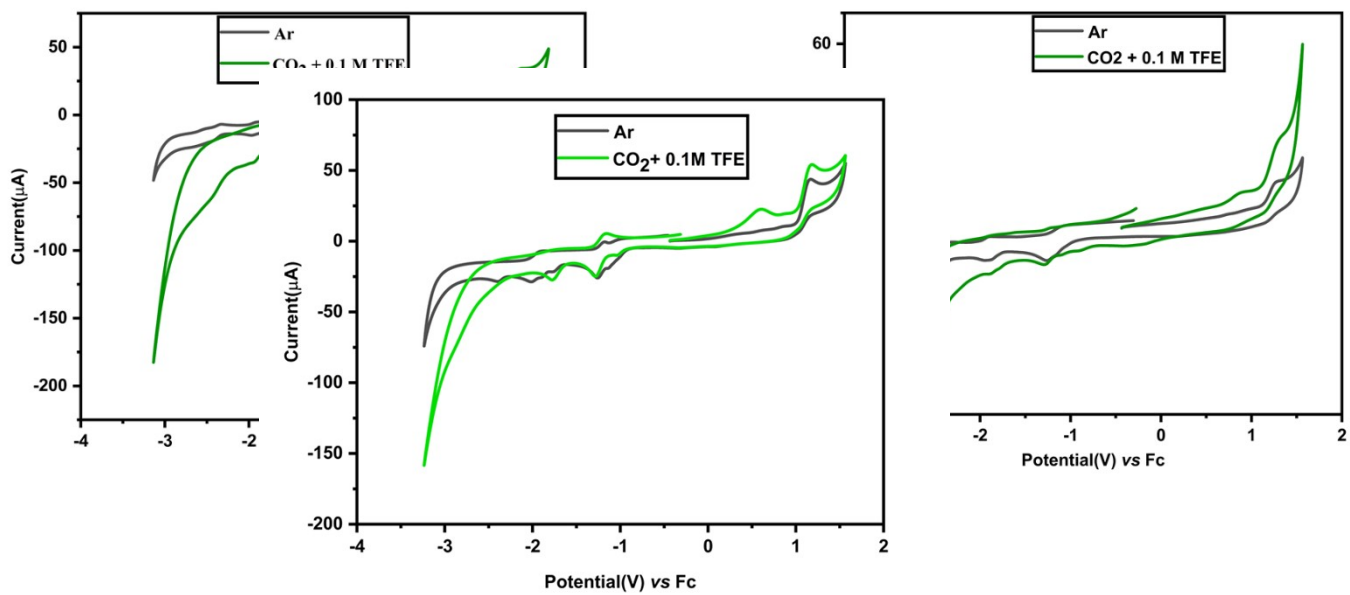


1c

2b

Fig. S28: Cyclic voltammograms of 1 mM solution of complexes 1a, 1b, 1c, 2a, 2b and 3a under Ar (black) and CO_2 atmosphere. Potential values are reported versus Fc^+/Fc .

Calculation of TOF_{max} for the Complexes:



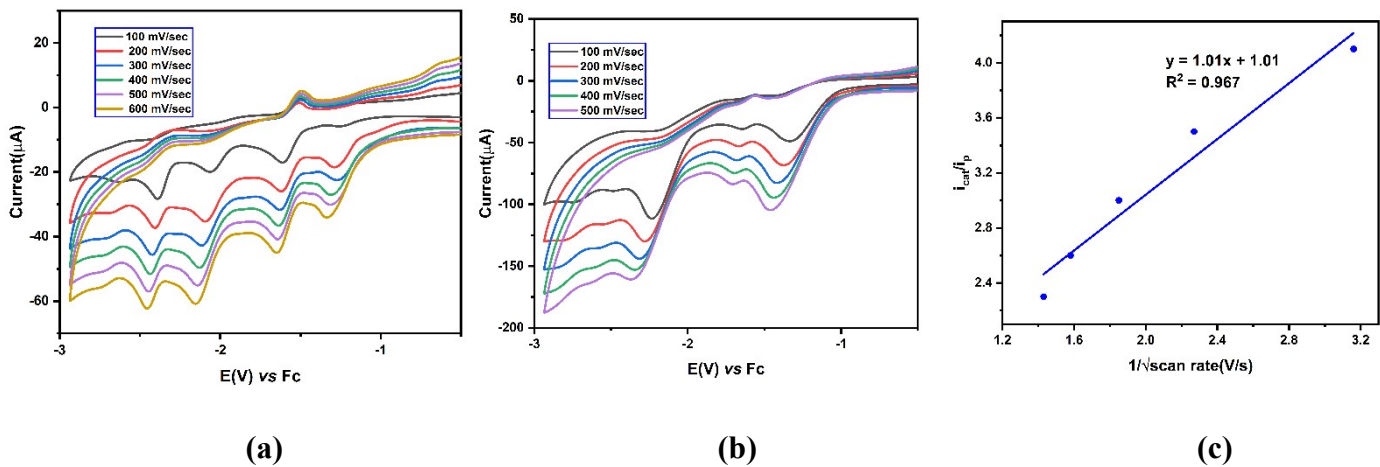


Fig. S29: Current vs. potential plot in different scan rate in Ar **(a)** and in presence of CO₂ **(b)**. i_p/i_{cat} vs. $1/\sqrt{\text{scan rate}^{1/2}}$ plot Complex 1a. Cyclic voltammogram scan rate dependence of 1 mM **complex-1a** under an atmosphere of argon **(a)** and under an atmosphere of CO₂ **(b)** in acetonitrile. **(c)** i_p/i_{cat} vs. $1/\sqrt{\text{scan rate}^{1/2}}$ plot of **complex-1a**. Electrochemical conditions were 0.1 M TBAH as supporting electrolyte, 3 mm diameter glassy carbon working electrode, Pt wire counter electrode, and Ag/AgCl reference electrode.

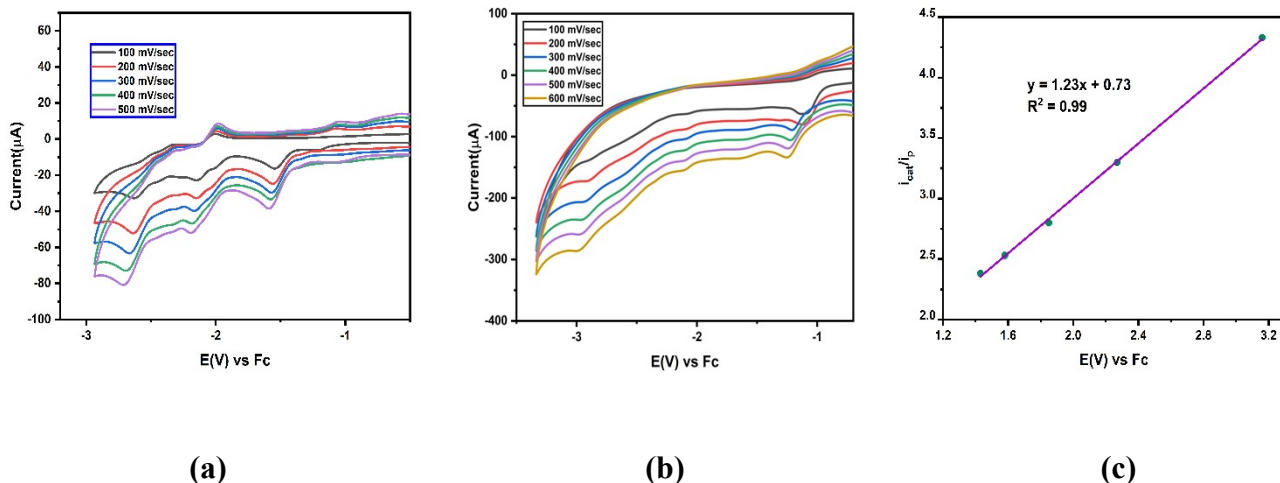


Fig. S30: Current vs. potential plot in different scan rate in Ar **(a)** and in presence of CO₂ **(b)**. i_p/i_{cat} vs. $1/\sqrt{\text{scan rate}^{1/2}}$ plot Complex 1a. Cyclic voltammogram scan rate dependence of 1 mM **complex-1b** under an atmosphere of argon **(a)** and under an atmosphere of CO₂ **(b)** in acetonitrile. **(c)** i_p/i_{cat} vs. $1/\sqrt{\text{scan rate}^{1/2}}$ plot of **complex-1b**. Electrochemical conditions were 0.1 M TBAH as supporting electrolyte, 3 mm diameter glassy carbon working electrode, Pt wire counter electrode, and Ag/AgCl reference electrode.

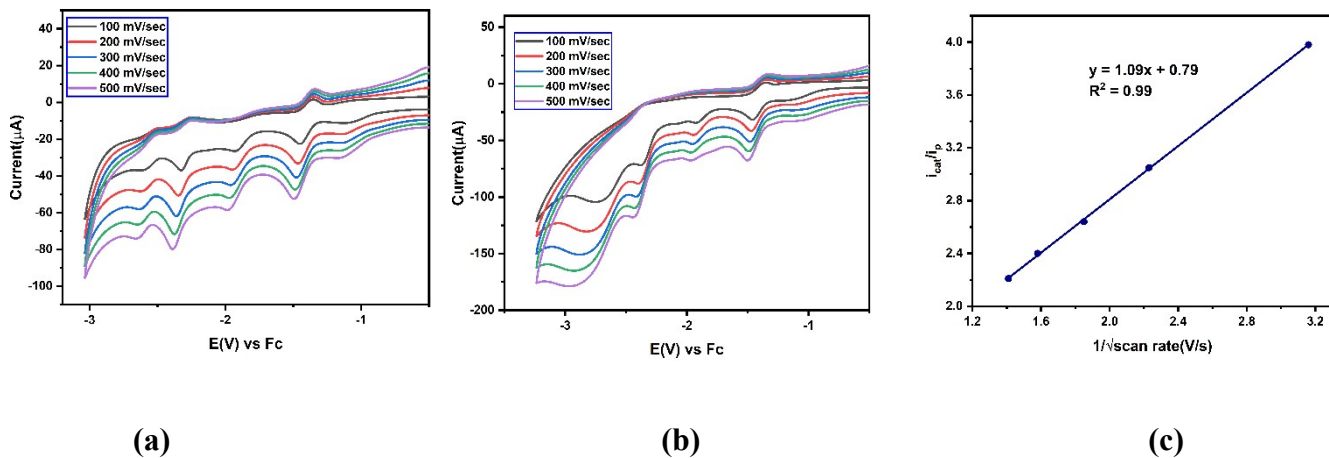


Fig. S31: Current vs. potential plot in different scan rate in Ar **(a)** and in presence of CO₂ **(b)**. i_p/i_{cat} vs. $1/\text{scan rate}^{1/2}$ plot Complex 1a. Cyclic voltammogram scan rate dependence of 1 mM **complex-1c** under an atmosphere of argon **(a)** and under an atmosphere of CO₂ **(b)** in acetonitrile. **(c)** i_p/i_{cat} vs. $1/\text{scan rate}^{1/2}$ plot of **complex-1c**. Electrochemical conditions were 0.1 M TBAH as supporting electrolyte, 3 mm diameter glassy carbon working electrode, Pt wire counter electrode, and Ag/AgCl reference electrode.

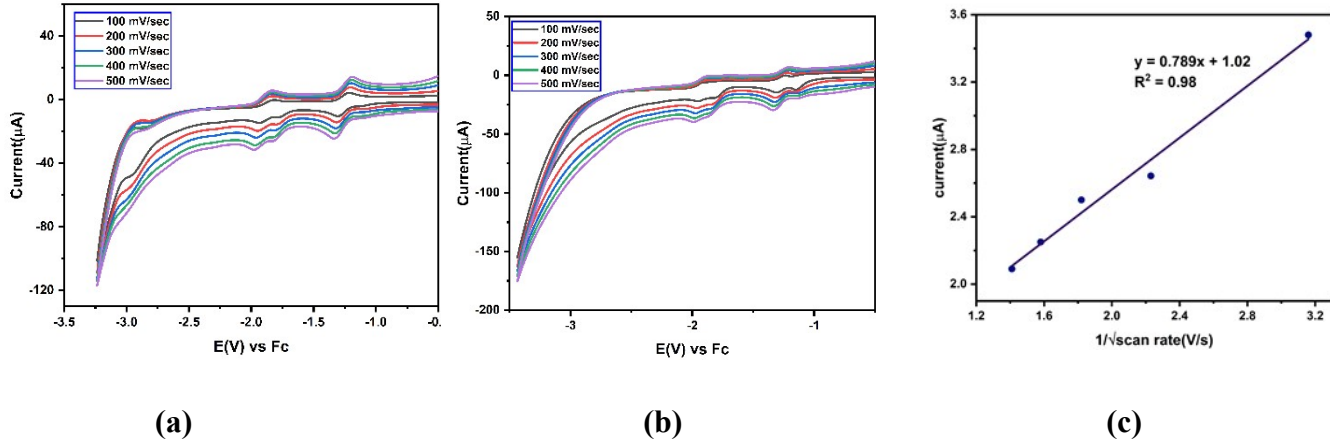


Fig. S32: Current vs. potential plot in different scan rate in Ar **(a)** and in presence of CO₂ **(b)**. i_p/i_{cat} vs. $1/\text{scan rate}^{1/2}$ plot Complex 1a. Cyclic voltammogram scan rate dependence of 1 mM **complex-2a** under an atmosphere of argon **(a)** and under an atmosphere of CO₂ **(b)** in acetonitrile. **(c)** i_p/i_{cat} vs. $1/\text{scan rate}^{1/2}$ plot of **complex-2a**. Electrochemical conditions were 0.1 M TBAH as supporting electrolyte, 3 mm diameter glassy carbon working electrode, Pt wire counter electrode, and Ag/AgCl reference electrode.

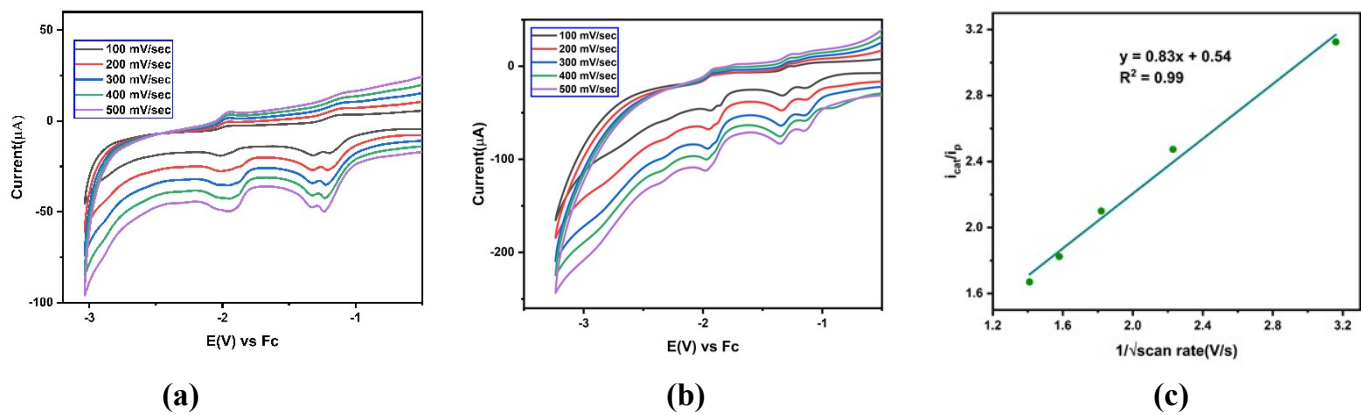


Fig. S33: Current vs. potential plot in different scan rate in Ar **(a)** and in presence of CO₂ **(b)**. i_p/i_{cat} vs. $1/\text{scan rate}^{1/2}$ plot Complex 1a. Cyclic voltammogram scan rate dependence of 1 mM **complex-2b** under an atmosphere of argon **(a)** and under an atmosphere of CO₂ **(b)** in acetonitrile. **(c)** i_p/i_{cat} vs. $1/\text{scan rate}^{1/2}$ plot of **complex-2b**. Electrochemical conditions were 0.1 M TBAH as supporting electrolyte, 3 mm diameter glassy carbon working electrode, Pt wire counter electrode, and Ag/AgCl reference electrode.

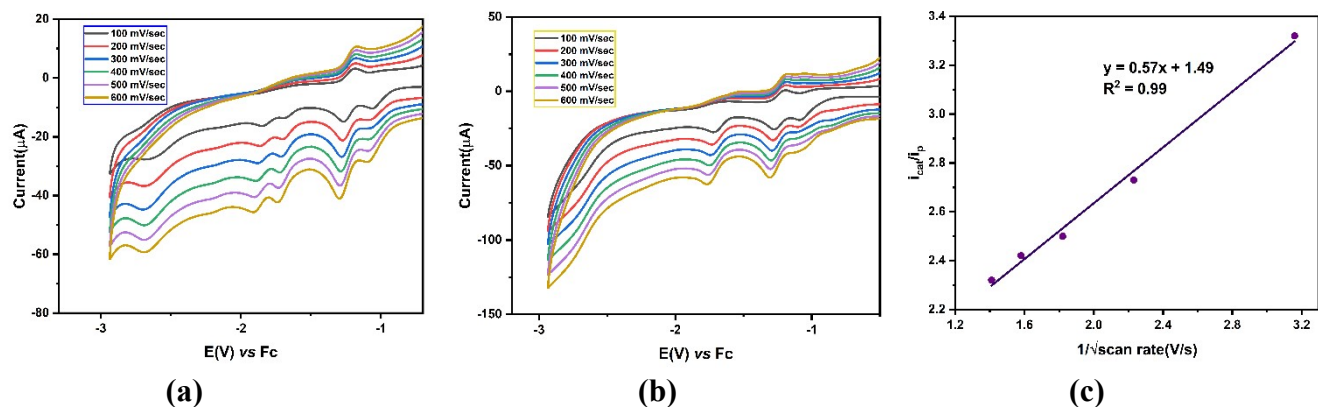


Fig. S34: Current vs. potential plot in different scan rate in Ar **(a)** and in presence of CO₂ **(b)**. i_p/i_{cat} vs. $1/\text{scan rate}^{1/2}$ plot Complex 1a. Cyclic voltammogram scan rate dependence of 1 mM **complex-3a** under an atmosphere of argon **(a)** and under an atmosphere of CO₂ **(b)** in acetonitrile. **(c)** i_p/i_{cat} vs. $1/\text{scan rate}^{1/2}$ plot of **complex-3a**. Electrochemical conditions were 0.1 M TBAH as supporting electrolyte, 3 mm diameter glassy carbon working electrode, Pt wire counter electrode, and Ag/AgCl reference electrode.

TOF_{max} calculations from the cyclic voltammetry experiments:

The turnover frequency (TOF) is an inherent characteristic of catalysts, which represents the rate of conversion reactants into products per mole of active catalyst per unit time. The TOF value was derived using the following equation below from the catalytic cyclic voltammograms recorded CH₃CN solutions.

$$TOF = (Fvn_p^3/RT)(0.4463/n_{cat})(i_{cat}/i_p)^2$$

Where, i_p is peak current, i_{cat} is the catalytic current, F is Faraday's constant (F = 96500 C), R is the universal gas constant (R = 8.314 J K⁻¹ mol⁻¹), T is temperature (T = 300 K) and v is the scan rate. (where n_p is 1, the number of electrons transferred in the noncatalytic reduction, and n_{cat} is 2 for CO₂ reduction to CO, the number of electrons transferred in the catalytic reaction). The TOF was calculated from the slope of i_{cat}/i_p vs $v^{-1/2}$ plot.

Catalyst	TOF _{max}
1a	1.80 s ⁻¹
1b	2.90 s ⁻¹
1c	2.28 s ⁻¹
2a	1.19 s ⁻¹
2b	1.32 s ⁻¹
3a	0.62 s ⁻¹

Table S8: TOF_{max} of the complexes in CH₃CN.

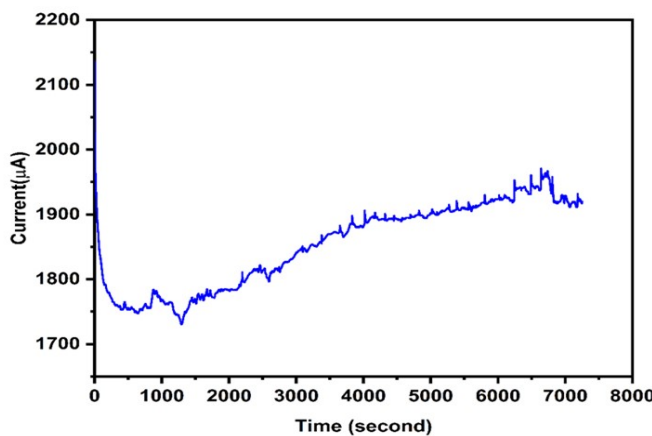


Fig. S35. Representative current versus time plots for controlled potential electrolyses of **Complex-1b**

Compound	Conc.(mM)	Faradaic efficiency (%)		
1b	1	H ₂	CO	CH ₄
		<1	33	6

Table S9. Faradaic efficiencies, in CH₃CN and 0.1M TFE after CPE experiments with a carbon working electrode for the complex 1b, for 2 hours at -2.5 V vs Ag/AgCl.



Fig. S36. GC-TCD data after controlled potential electrolyses.

No.	Solvent(4ml)	Electron donor	λ (nm)	Gas	Reduced products		TON _{CO}
					CO (μmol)	H ₂ (μmol)	
1	DMF/H ₂ O(4:1)	BIH	$420 \leq \lambda \leq 750$	CO ₂	42	0.012	420
2	DMF/TEOA(4:1)	BIH	$420 \leq \lambda \leq 750$	CO ₂	26	3.03	260
3	DMA/H ₂ O(4:1)	BIH	$420 \leq \lambda \leq 750$	CO ₂	33	0.01	330
4	DMF/TEA(4:1)	BIH	$420 \leq \lambda \leq 750$	CO ₂	5	2.88	50
5	CH ₃ CN/H ₂ O(4:1)	BIH	$420 \leq \lambda \leq 750$	CO ₂	9	<0.01	90
6	CH ₃ CN/TEOA(4:1)	BIH	$420 \leq \lambda \leq 750$	CO ₂	37	0.01	370
7	CH ₃ CN/TFE(4:1)	BIH	$420 \leq \lambda \leq 750$	CO ₂	22	<0.01	220

8	DMF/TFE(4:1)	BIH	$420 \leq \lambda \leq 750$	CO ₂	27	1.32	270
9	CH ₃ CN/TEOA(4:1)	BIH	Dark	CO ₂	0	0	0
10	CH ₃ CN/TEOA(4:1)	BIH	$420 \leq \lambda \leq 750$	N ₂	0	0	0
11	CH ₃ CN/TEOA(4:1) + 0.1 ml TFE	BIH	$420 \leq \lambda \leq 750$	CO ₂	33	0.2	330

Table S10. Photocatalytic CO₂ reduction at different condition. For all catalysts, the photochemical conditions include 4 mL of solvent, 0.2 mM Ru(dmbpy)₃²⁺ as the photosensitizer, 25 mM SED, and 20 μ M complex-1a. The quantities of the reduced products generated by the catalysts were measured after 2 hours.

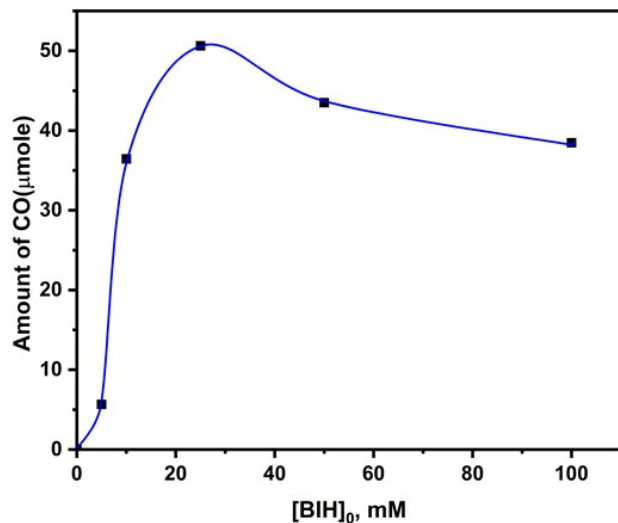
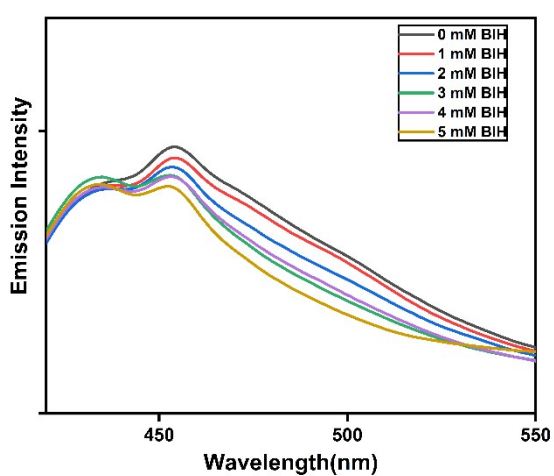
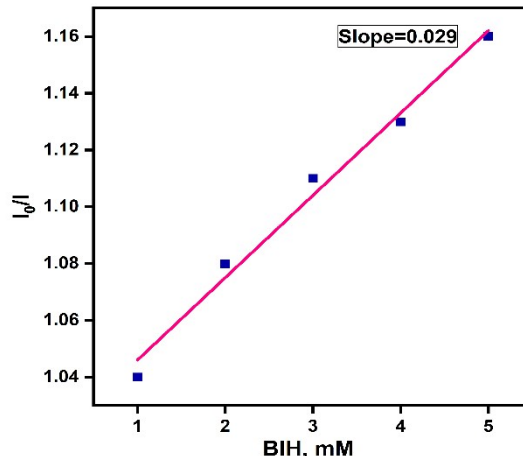


Fig. S37. The amount of CO produced after 4 hours of photocatalytic CO₂ reduction by complex-1a as a function of BIH concentration.



(a)



(b)

Fig. S38. (a) Emission spectra of Complex-**1a** (20 μ M) excited by monochromatic light at 400 nm CH_3CN containing BIH (0 – 5 mM) at 298 K. (b) A Stern-Volmer plots for the emission quenching by BIH (0 – 5 mM).

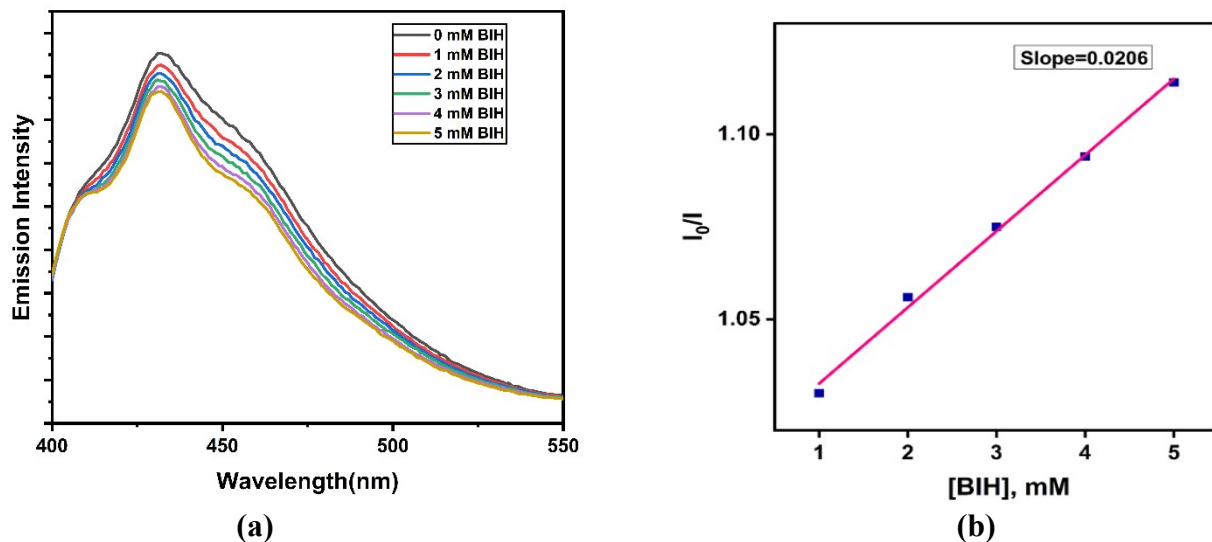


Fig. S39. (a) Emission spectra of Complex-**1b** (20 μ M) excited by monochromatic light at 400 nm CH_3CN containing BIH (0 – 5 mM) at 298 K. (b) A Stern-Volmer plots for the emission quenching by BIH (0 – 5 mM).

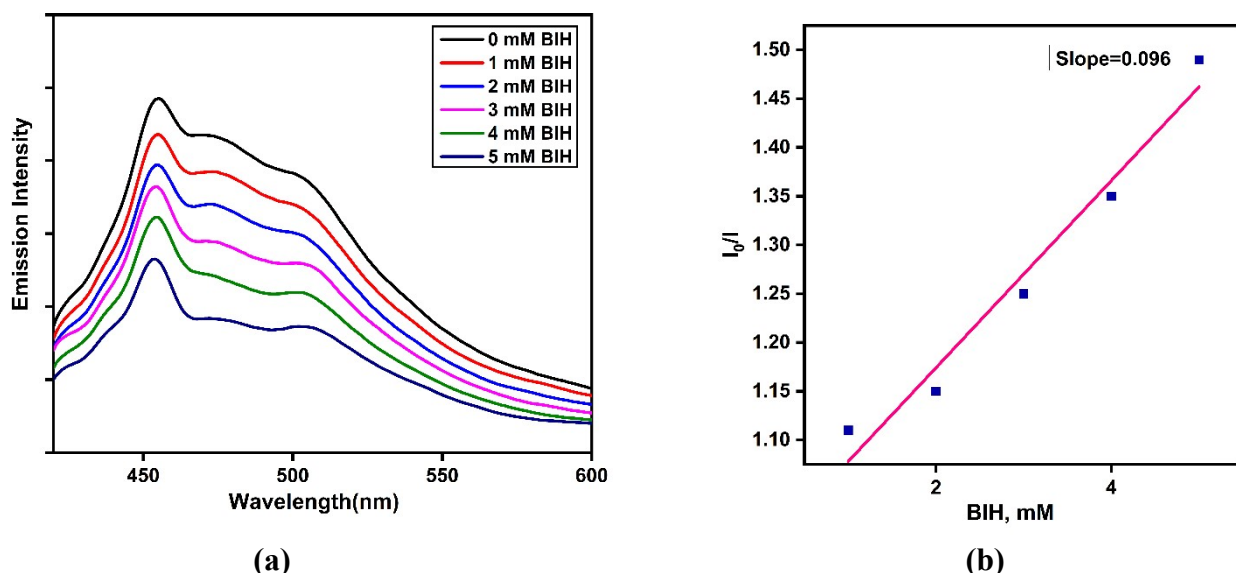


Fig. S40. (a) Emission spectra of Complex-**1c** (20 μ M) excited by monochromatic light at 402 nm CH_3CN containing BIH (0 – 5 mM) at 298 K. (b) A Stern-Volmer plots for the emission quenching by BIH (0 – 5 mM).

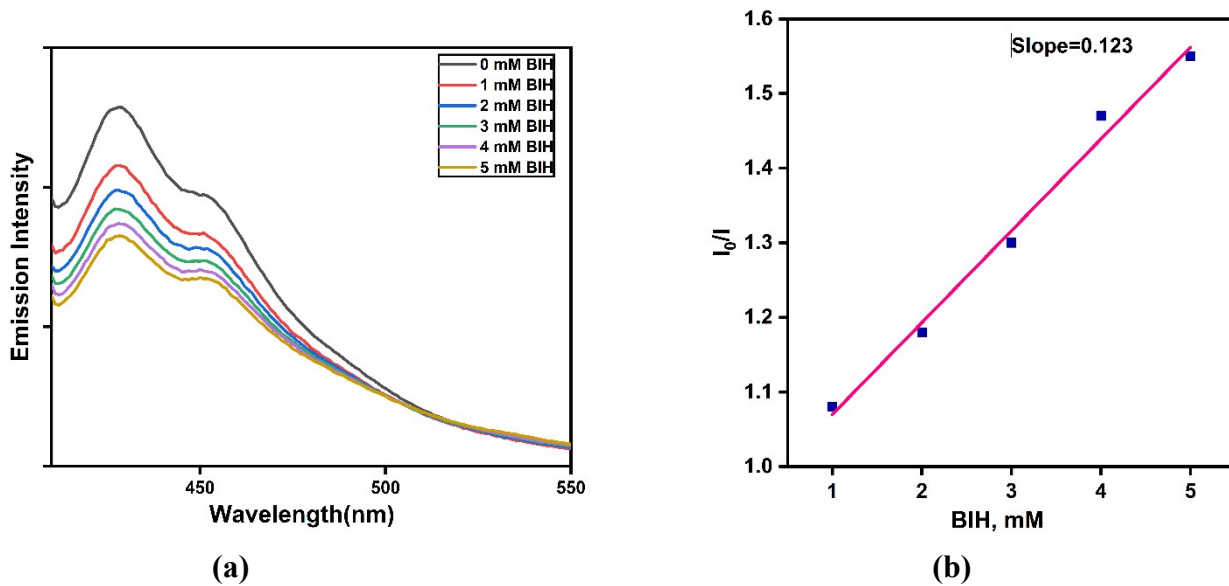


Fig. S41. (a) Emission spectra of Complex-**2a** (20 μ M) excited by monochromatic light at 400 nm CH_3CN containing BIH (0 – 5 mM) at 298 K. (b) A Stern-Volmer plots for the emission quenching by BIH (0 – 5 mM).

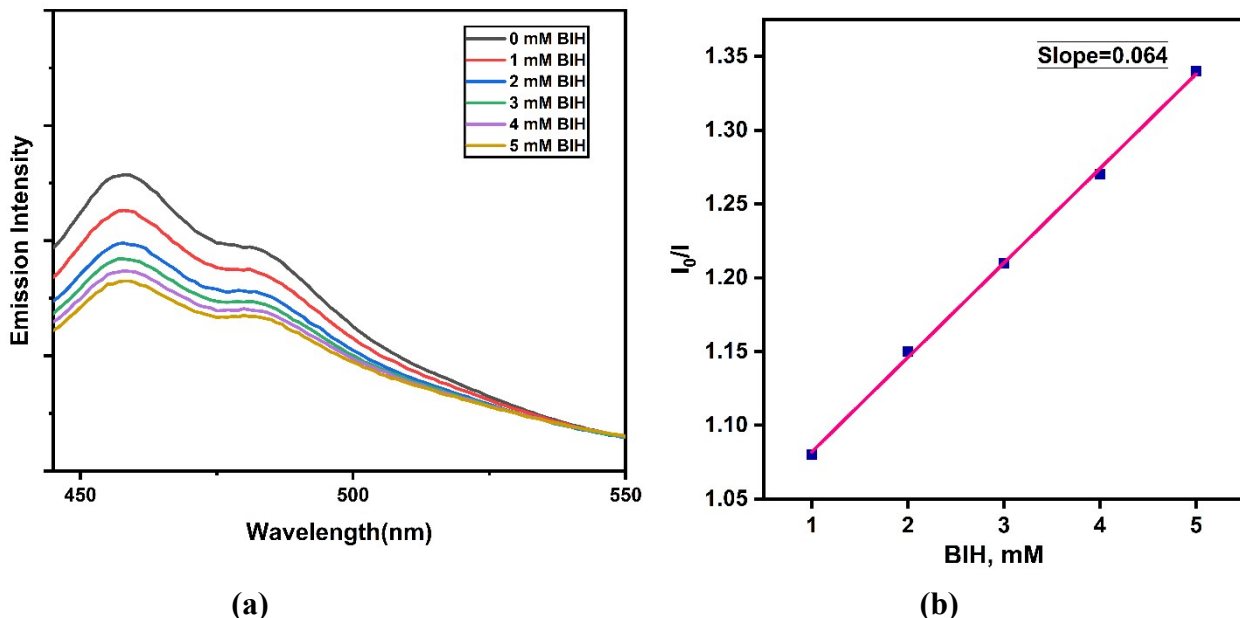
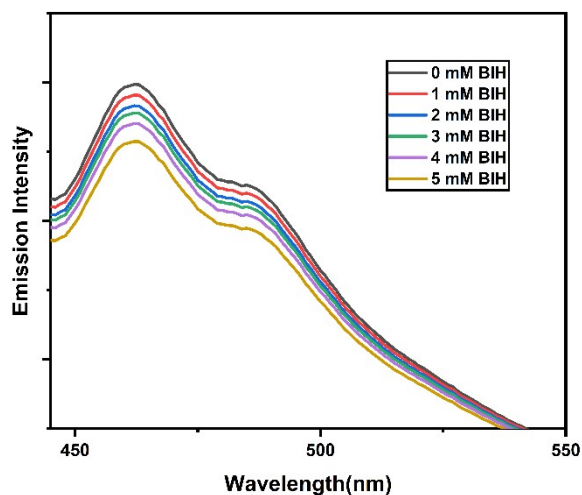
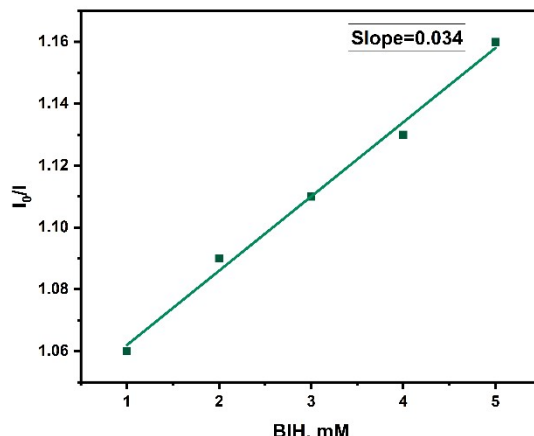


Fig. S42. (a) Emission spectra of Complex-**2b** (20 μ M) excited by monochromatic light at 416 nm CH_3CN containing BIH (0 – 5 mM) at 298 K. (b) A Stern-Volmer plots for the emission quenching by BIH (0 – 5 mM).



(a)



(b)

Fig. S43. (a) Emission spectra of Complex-3a (20 μ M) excited by monochromatic light at 430 nm CH_3CN containing BIH (0 – 5 mM) at 298 K. (b) A Stern-Volmer plots for the emission quenching by BIH (0 – 5 mM).

Catalyst	$K_{\text{SV}}(\text{L mol}^{-1})$	$k_{\text{q}}(10^9 \text{ L mol}^{-1} \text{ s}^{-1})$
1a	29.0	6.9
1b	20.6	9.7
1c	96.0	18.2
2a	123	17.4
2b	64	31.6
3a	34	6.4

Table S11: Stern–Volmer Constants (K_{SV}), Reductive Quenching Rate Constants (k_{q}) by BIH for the catalysts.

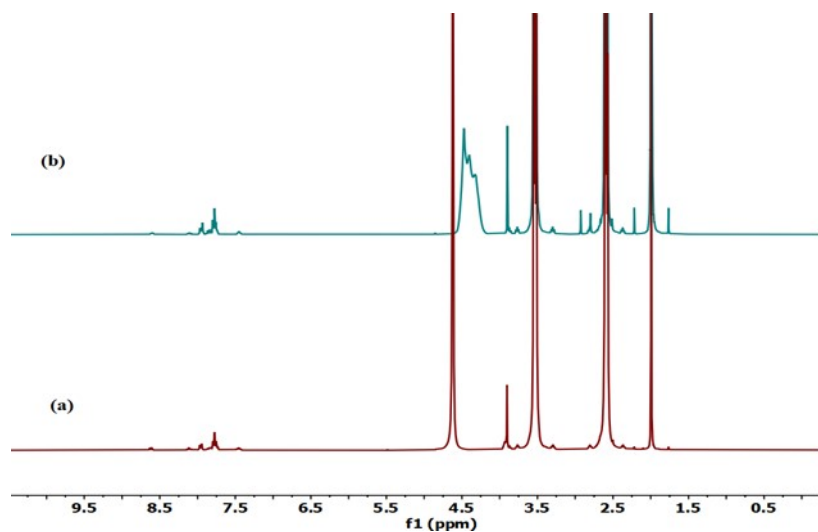


Fig. S44: ¹H NMR spectra in CD₃CN/TEOA in the presence of BIH, SP under CO₂ atmosphere and



photo irradiation $\lambda \geq 400$ nm , irradiation time 5 hours (a), without catalyst (b) with catalyst

Fig. S45: Photocatalytic reduction of CO₂ in bare sunlight by Complex **1a, 2a and 3a**.

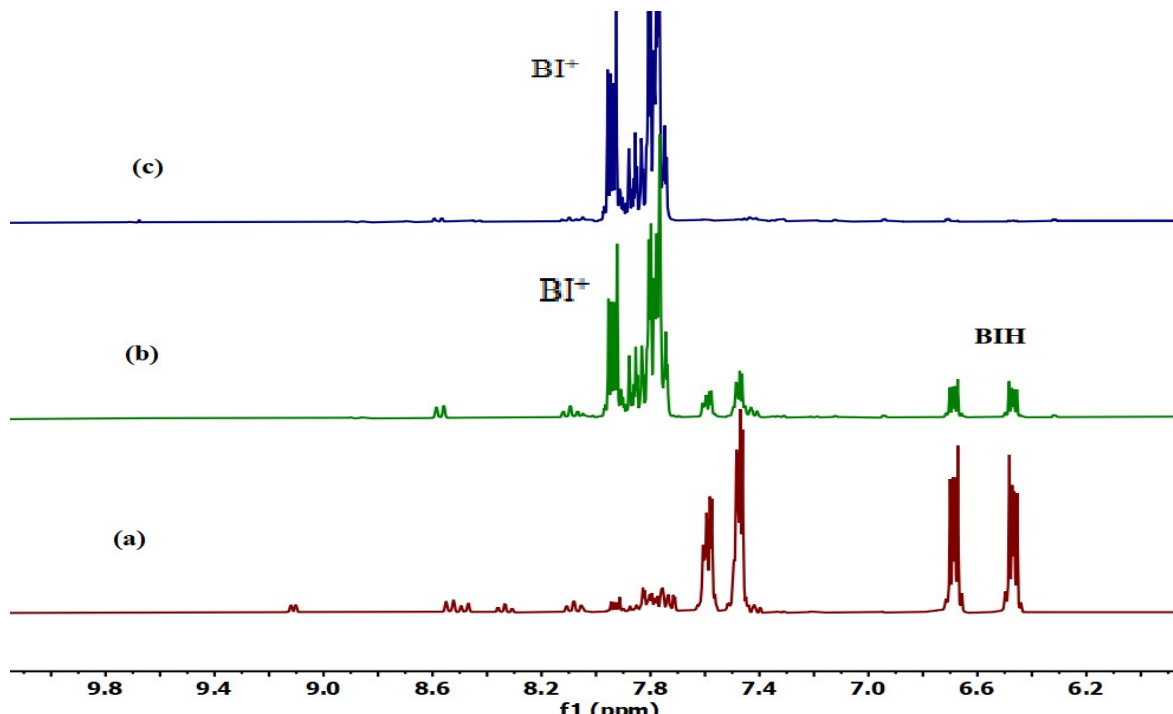
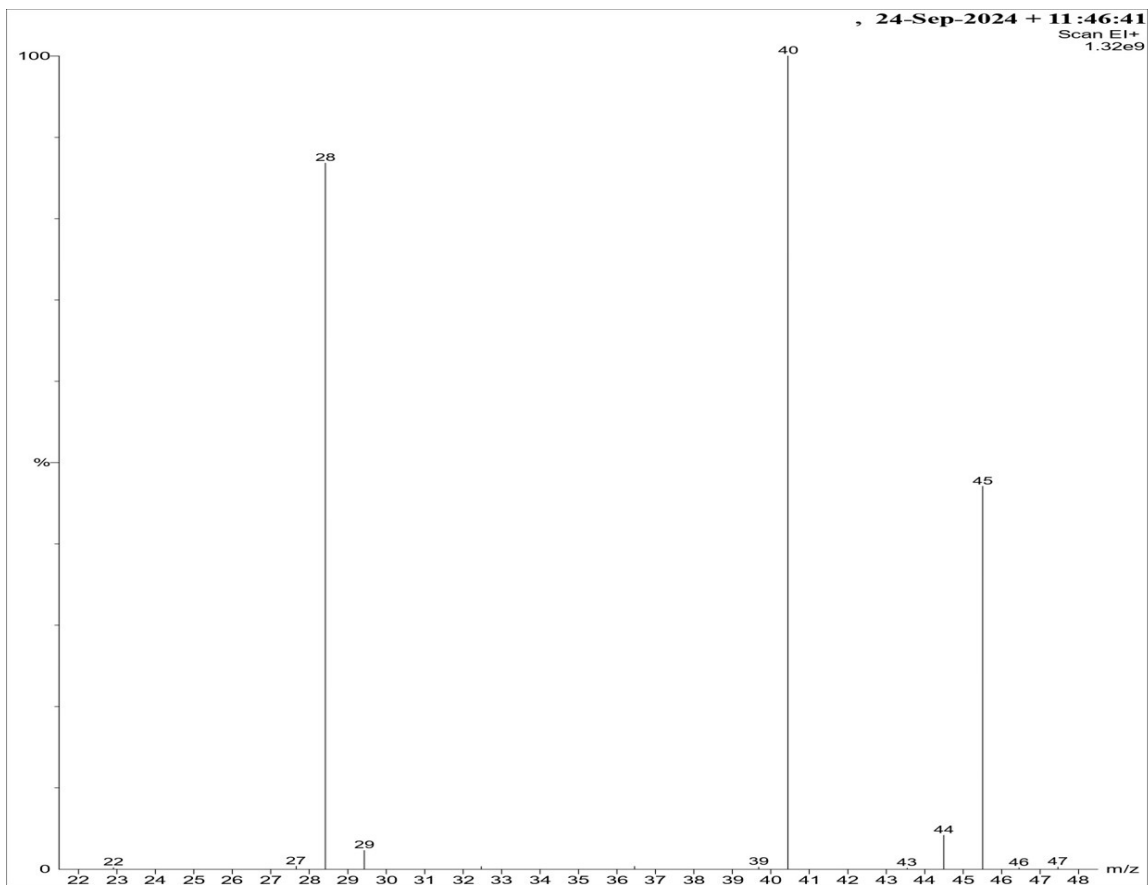


Fig. 46: Mass spectra obtained from GC-MS analysis using labelled $^{13}\text{CO}_2$.

Fig. S47: ^1H NMR spectra of **Complex-1b** in $\text{CD}_3\text{CN}/\text{TEOA}$ in the presence of BIH and PS under CO_2 atmosphere and photo irradiation $\lambda \geq 400 \text{ nm}$, irradiation time 0 min. (a), 60 min (b) 120 min(c)

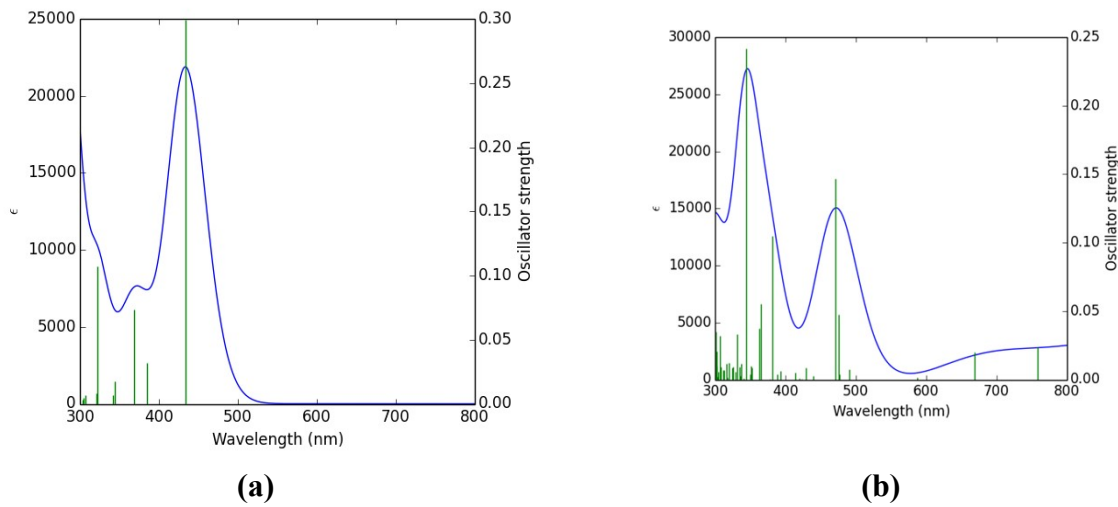


Fig. 48: TD-DFT calculation of **Complex-1b** (a) and its one electron reduced state (b).

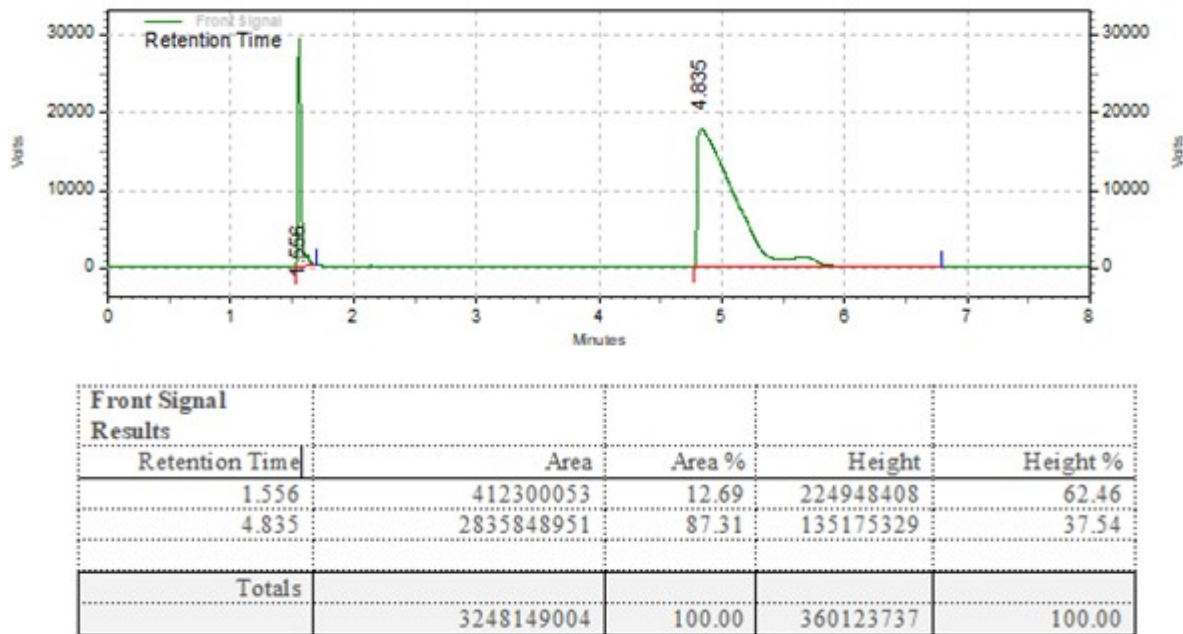


Fig. 49: GC-TCD data for detection and amount calculation for CO.

References:

1. SMART; SAINT; SADABS; XPREP; SHELXTL, Bruker AXS Inc., Madison, WI, 1998.
2. G. M. Sheldrick, SHELXTL, v. 6.14, Bruker AXS Inc., Madison, WI, 2003.
3. E. Runge and E. K. U. Gross, *Phys. Rev. Lett.*, 1984, **52**, 997–1000.
4. (a) A. D. Becke, *J. Chem. Phys.*, 1993, **98**, 5648–5652; (b) C. Lee, W. Yang and R. G. Parr, *Phys. Rev. B: Condens. Matter*, 1988, **37**, 785–789.
5. (a) M. E. Casida, C. Jamoroski, K. C. Casida and D. R. Salahub, *J. Chem. Phys.*, 1998, **108**, 4439–4449; (b) R. E. Stratmann, G. E. Scuseria and M. J. Frisch, *J. Chem. Phys.*, 1998, **109**, 8218–8224; (c) R. Bauernschmitt and R. Ahlrichs, *Chem. Phys. Lett.*, 1996, **256**, 454–464.
6. (a) V. Barone and M. Cossi, *J. Phys. Chem. A*, 1998, **102**, 1995–2001; (b) M. Cossi and V. Barone, *J. Chem. Phys.*, 2001, **115**, 4708–4717; (c) M. Cossi, N. Rega, G. Scalmani and V. Barone, *J. Comput. Chem.*, 2003, **24**, 669–681.
7. (a) T. Liu, H.-X. Zhang and B.-H. Xia, *J. Phys. Chem. A*, 2007, **111**, 8724–8730; (b) X. Zhou, H.-X. Zhang, Q.-J. Pan, B.-H. Xia and A.-C. Tang, *J. Phys. Chem. A*, 2005, **109**, 8809–8818; (c) X. Zhou, A.-M. Ren and J.-K. Feng, *J. Organomet. Chem.*, 2005, **690**, 338–347; (d) A. Albertino, C. Garino, S. Ghiani, R. Gobetto, C. Nervi, L. Salassa, E. Rosenverg, A. Sharmin, G. Viscardi, R. Buscaino, G. Cross and M. Milanesio, *J. Organomet. Chem.*, 2007, **692**, 1377–1391.
8. (a) P. J. Hay and W. R. Wadt, *J. Chem. Phys.*, 1985, **82**, 270–283; (b) P. J. Hay and W. R. Wadt, *J. Chem. Phys.*, 1985, **82**, 299–310.
9. M. J. Frisch, G. W. Trucks, H. B. Schlegel, G. E. Scuseria, M. A. Robb, J. R. Cheeseman, G. Scalmani, V. Barone, B. Mennucci, G. A. Petersson, H. Nakatsuji, M. Caricato, X. Li, H. P. Hratchian, A. F. Izmaylov, J. Bloino, G. Zheng, J. L. Sonnenberg, M. Hada, M. Ehara, K. Toyota, R. Fukuda, J. Hasegawa, M. Ishida, T. Nakajima, Y. Honda, O. Kitao, H. Nakai, T. Vreven, J. A. Montgomery Jr., J. E. Peralta, F. Ogliaro, M. Bearpark, J. J. Heyd, E. Brothers, K. N. Kudin, V. N. Staroverov, R. Kobayashi, J. Normand, K. Raghavachari, A. Rendell, J. C. Burant, S. S. Iyengar, J. Tomasi, M. Cossi, N. Rega, J. M. Millam, M. Klene, J. E. Knox, J. B. Cross, V. Bakken, C. Adamo, J. Jaramillo, R. Gomperts, R. E. Stratmann, O. Yazyev, A. J. Austin, R. Cammi, C. Pomelli, J. W. Ochterski, R. L. Martin, K. Morokuma, V. G. Zakrzewski, G. A. Voth, P. Salvador, J. J. Dannenberg, S. Dapprich, A. D. Daniels, Ö. Farkas, J. B. Foresman, J. V. Ortiz, J. Cioslowski and D. J. Fox, GAUS-SIAN 09 (Revision A.1), Gaussian, Inc., Wallingford, CT, 2009.

